Ocean acidification enhances primary productivity and nocturnal carbonate dissolution in intertidal rock pools

Narimane Dorey[1, †], Sophie Martin[2, 3], Lester Kwiatkowski[4]

[1] LMD-IPSL, CNRS, ~~Ecole~~École Normale Supérieure/PSL Res. Univ, ~~Ecole~~École Polytechnique, Sorbonne Université, Paris, 75005, France

[2] CNRS, UMR7144, Station Biologique, Place Georges Teissier, 29688 Roscoff Cedex, France

[3] Laboratoire Adaptation et Diversité en Milieu Marin, Sorbonne Universités, UPMC Univ Paris 06, Station Biologique, Place Georges Teissier, 29688 Roscoff Cedex, France

[4] LOCEAN Laboratory, Sorbonne Université-CNRS-IRD-MNHN, Paris, 75005, France

[†] Correspondence to: Narimane Dorey

~~Ecole~~École Normale Supérieure,

Département de Géosciences,

24 rue Lhomond, 75005 Paris, France

E-mail: narimane.dorey@gmail.com

Formatted: English (US)

ABSTRACT

Human CO_2 emissions are modifying ocean carbonate chemistry, causing ocean acidification, and likely already impacting marine ecosystems. In particular, there is concern that coastal, benthic calcifying organisms will be negatively affected by ocean acidification, a hypothesis largely supported by laboratory studies. The inter-relationships between carbonate chemistry and marine calcifying communities *in situ* are complex and natural mesocosms such as tidal pools can provide useful community-level insights. In this study, we manipulated the carbonate chemistry of intertidal pools to investigate the influence of future ocean acidification on net community production (NCP) and calcification (NCC) at emersion. Adding CO_2 at the start of the tidal emersion to simulate future acidification ($+1500$ μatm pCO_2, target pH: 7.5) modified net production and calcification rates in the pools. By day, pools were fertilized by the increased CO_2 ($+20$ % increase in NCP, from 10 to 12 mmol O_2 m^{-2} hr^{-1}), while there was no measurable impact on NCC. During the night, pools experienced net community dissolution (NCC < 0), even in present-day conditions, when waters were supersaturated with regards to aragonite. Adding CO_2 in the pools increased nocturnal dissolution rates by 40% (from -0.7 to -1.0 mmol $CaCO_3$ m^{-2} hr^{-1}) with no consistent impact on night community respiration. Our results suggest that ocean acidification is likely to alter temperate intertidal community metabolism on sub-daily timescales, enhancing both diurnal community production and nocturnal calcium carbonate dissolution.

SHORT SUMMARY

Human CO_2 emissions are modifying ocean carbonate chemistry, causing ocean acidification, and likely already impacting marine ecosystems. Here, we added CO_2 in intertidal pools at the start of emersion to investigate the influence of future ocean acidification on net community production (NCP) and calcification (NCC). By day, adding CO_2 fertilized the pools ($+20$ % NCP). By night, pools experienced net community dissolution, a dissolution that was further increased ($+40$ %) by the CO_2 addition.

Keywords: Ocean acidification, calcification, coralline algae, mesocosms, primary production, temperate community, tidal pool

INTRODUCTION

The ongoing increase of anthropogenic carbon dioxide (CO_2) in the atmosphere and the ocean – resulting in ocean acidification - is likely to create adverse living conditions for marine coastal communities (IPCC, 2019). Ocean acidification is projected to further decrease average surface pH by up to 0.4 units by 2100 (scenario RCP8.5, Kwiatkowski et al., 2020), and is identified as a major threat to marine ecosystems (IPCC, 2019). Lower seawater pH has significant effects on marine organisms physiology and fitness: from altered survival and reduced growth (see review by Kroeker et al. 2013), to changes in pH homeostasis (e.g., Kottmeier et al., 2022), metabolic rates, and energy trade-offs (e.g., Dorey et al., 2013; Pan et al., 2015) and reduced feeding efficiency (e.g., Stumpp et al., 2013). Marine calcifiers - the builders of calcified structures ($CaCO_3$) - have been a focus of ocean acidification research due to the sensitivity of calcification to the carbonate saturation state (Ω), defined as follows:

$$\Omega = [Ca^{2+}] \, [CO_3^{2-}]/K'_{sp}$$

where K'$_{sp}$ is the stoichiometric solubility product for the considered carbonate polymorph (i.e., Ω_a for aragonite or Ω_c for calcite). The saturation state depends on temperature, pH, and pressure (lower Ω when pH or temperature decreases and pressure increases). When $\Omega < 1$, inert carbonate minerals tend to dissolve. The polymorphs composing the calcified structure like calcite and to a greater extent aragonite and high-magnesium calcite, are prone to dissolution when pH decreases. For instance, in Atlantic surface waters (at 20°C), saturation state equilibrium ($\Omega = 1$) is reached at pH 7.3 (pCO_2 = 2650 µatm) for calcite but at pH 7.6 (1250 µatm) for aragonite. For high-magnesium calcite, experiments from (Yamamoto et al., 2012) demonstrate that inert (dead) high-magnesium calcite from coralline algae passively dissolves at Ω_a values between 3.0 and 3.2 (also see Ries et al. 2016). Organisms with calcified structures are thus likely to experience reduced net calcification due to ocean acidification, both through enhanced dissolution, and reduced gross calcification rates.

Aside from acidifying the ocean (increased H^+), increased ocean CO_2 uptake could affect the productivity of algae and marine plants. As CO_2 dissolves in the ocean, the dissolved inorganic carbon (DIC: CO_2, HCO_3^- and CO_3^{2-}) concentration increases. DIC is the substrate for marine photosynthesis (mainly CO_2 and HCO_3^-), and as such, it can limit photosynthetic rates when scarce.

75   In algae and marine plants that are carbon limited (permanently or periodically), elevated DIC
76   could also directly increase photosynthetic rates and Mackey et al., (2015) propose that these rates
77   could be further increased by the higher concentration gradient between water and the
78   photosynthetic cells. However, the authors point out that while positive effects are theoretically
79   expected, they may be small, specific to species' biology and the environment they live in, and
80   difficult to predict (see also Hurd et al., 2019). In terrestrial ecosystems, the Intergovernmental
81   Panel on Climate Change defines CO_2 fertilization as 'the enhancement of plant growth as a result
82   of increased atmospheric CO_2 concentration' (Jia et al., 2019) and reports that CO_2 fertilization
83   has likely already happened, although the magnitude of this effect depends on the plants, or
84   assemblages/ecosystems considered (and on other factors constraining growth).

85   The response of single species to changes such as ocean acidification and increased DIC
86   concentrations are often insufficient to predict community-level impacts. Ecological interactions
87   such as competition or predation can affect the outcome of perturbation experiments (Kroeker et
88   al., 2012). For instance, Paiva et al. (2021) showed that the laboratory growth of an isopod species
89   was an order of magnitude slower than when raised in the presence of other species from its
90   community. In another study, Legrand et al. (2019) showed that the presence of grazers increased
91   coralline algal calcification (+50% in winter and +100% in summer), but when grazers were
92   combined with ocean acidification, algal calcification decreased more than with acidification
93   alone. Not taking into account such interactions can therefore result in poorly characterizing the
94   effects of ocean acidification. Furthermore, while critical for a mechanistic understanding of the
95   processes affecting marine biota, laboratory studies are seldom realistic. Typically performed in
96   controlled, simplified, and stable conditions (e.g., with respect to temperature and food), laboratory
97   studies can better assess the effect of pH alone (Widdicombe et al., 2010). However exposure to a
98   stable pH (e.g., 7.6 vs. 8.0), fails to reflect the daily and seasonal variability observed in natural
99   ecosystems, in particular coastal ones (Torres et al., 2021). Natural mesocosm perturbation
100 experiments are thus essential tools to investigate future changes in variable and complex
101 ecosystems, difficult to capture in the lab (Andersson et al., 2015; Barry et al., 2010).

102   Most *in situ* mesocosm experiments investigating the effect of ocean acidification have
103 been conducted on planktonic communities, kept in large "bags" equilibrated to the desired pH
104 (Riebesell et al., 2013). These studies demonstrate that adding CO_2 can significantly change the

105   organization of the plankton community (Spisla et al., 2021), and increase autotrophic biomass in

106   high-nutrient conditions (Schulz et al., 2013). Due to the technical challenges, however, benthic

107   calcifying communities are seldom manipulated this way *in situ* (Widdicombe et al., 2010). Two

108   such manipulation experiments are the studies by Albright et al. (2016, 2018), where the authors

109   used NaOH and CO_2 to reproduce pre-industrial and future pH conditions on a coral reef and found

110   evidence that reef growth had been reduced by 7% over the industrial era and was likely to decline

111   further. Other studies have investigated such community-level effects by either simulating

112   "artificial", simpler, assemblages in laboratory setups (e.g., Cox et al., 2015; Pansch et al., 2016)

113   or using phenomena such as natural CO_2 vents. For instance, in the vents of Ischia, as pH decreases,

114   the presence of calcifying species declines (see review by Foo et al., 2018). Alternatively,

115   Kwiatkowski et al. (2016) used locally-induced acidification due to respiration (no CO_2 addition)

116   in tidal pools, a naturally closed system, and demonstrated that nighttime dissolution of these

117   communities was positively correlated with Ω. Here, we used tidal pools of the English Chanel as

118   ephemeral mesocosms, where we modified carbonate chemistry conditions at the start of emersion

119   through CO_2 addition.

120   Temperate rocky tidal pools - or rockpools - are highly dynamic systems that have been long

121   studied by naturalists since they are easy to reach and their ecosystem structure generally resemble

122   subtidal benthic communities (Ganning, 1971). Tidal pool organisms from the upper shore, well-

123   adapted to pool conditions, form typical benthic communities: often low in diversity, they consist

124   of a few characteristic macroalgal (e.g., *Ulva sp.*) and animal species (e.g., limpets). In winter, red

125   macroalgae – including calcifying algae – often dominate the pools and while they do not disappear

126   in summer, a bloom of soft green macroalgae is generally observed during the warm season.

127   Temperature, salinity, oxygen, and pH in the pools are extremely variable, often far outside the

128   seasonal range of nearby free-flowing seawater (Legrand et al., 2018; Morris & Taylor, 1983).

129   Tidal pools generally emerge from the ocean twice a day in regions of semidiurnal tides with the

130   duration dependent on shore location and the tidal coefficient. On short timescales tidal pools act

131   as closed systems, with carbonate chemistry easily manipulated and temporal changes reflecting

132   *in situ* community metabolism (no water mass transport and negligible air-sea gas exchange).

133   In the present study, we used tidal pools as natural mesocosms to investigate the effect of ocean

134   acidification on communities dominated by calcifying red algae. We measured diurnal and

135 nocturnal net community calcification and production (or respiration) following CO_2 addition
136 across three seasons (winter, spring, and summer), to assess how tidal pool community metabolism
137 may respond to end of the 21st century high ocean acidification (pH 7.5).

138

MATERIAL AND METHODS

Field site

141 The experiments were performed on a rocky intertidal shore characterized by granitic substrate on
142 the North coast of Brittany, France, between 2019 and 2021. The beach of Bloscon (48°43'30.0"N
143 3°58'10.5"W) is situated in Roscoff at the entrance of the Bay of Morlaix and has a hydrology
144 principally affected by the waters of the English Channel and to a lesser extent the Penzé and
145 Morlaix rivers (**Fig. 1**). This area is characterized by strong, oscillating, semidiurnal tides of up to
146 9 m. Temperatures are generally low in the deeper flowing water (from 9-10 °C in winter to 16-17
147 °C in summer), and salinity is close to that of the adjacent Atlantic (~35; see **Supp. Mat. Fig. S1**
148 for detailed temperature and salinity data from the two nearby SOMLIT monitoring stations
149 Estacade and Astan, a network described in Cocquempot et al., 2019).

Tidal pool characterization

151 For this study, we chose five tidal pools with high coverage in calcifying algae (≥ 30% of the pool
152 surface area). Both crustose (CCA) and articulated (branching) coralline algae (ACA) were
153 present. The field site has an eastern exposure, resulting in full morning sun and relatively early
154 shade in the evening. Foreshore locations of the pools resulted in daily emersion year-round
155 including during neap tides (mid-tide, approx. 5-6 m above chart datum). Pools emerged for 6-7 h
156 during low-tide periods. During that time, pools were completely separated from the adjacent open
157 water and their depths were effectively constant in winter (low-evaporation season), an indication
158 that there was no seawater leakage.

159 The volume of each of the five pools (from 16 to 39 L; **Fig. 2**) was estimated in April 2021
160 at the end of the emersion period just before high-tide flooding, by measuring salinity changes
161 when a known volume of freshwater was added and well mixed. To estimate the pools' initial
162 volumes, we also took into consideration the measured salinity changes throughout the emersion

period to estimate evaporative losses and combined this with the volume directly lost through water sampling (see below). The pool projected area and the relative area covered by each type of algae were estimated from aerial photographs, with a scale and analyzed using ImageJ (U. S. National Institutes of Health, Bethesda, Maryland, USA, *https://imagej.nih.gov/ij*). Pool area ranged from 0.3 to 0.67 m^2 (**Fig. 2**). The pools had slightly different community composition with dominant calcifying red algae represented by *Lithophyllum incrustans* (CCA: 30 to 7177 % of the benthic cover) and *Ellisolandia elongata* (ACA: 0 to 6 % of the benthic cover). The remaining pool area was either free of algal cover with only bare granitic rock visible or covered by soft macroalgae. In summer (September 2020 and 2021), the pools also hosted the green algae *Ulva sp.* and *Enteromorpha sp.* (2 to 44 % of the benthic cover: see **Supp. Mat. Pools: Fig. SP1-2,** for results detailed by season) and, in Pool E, small single branches of the brown algae *Sargassum muticum*, covering less than 0.5 % of the pool. One limit of this method of aerial photography is that it only takes into account what is visible from above (2D). These estimates may thus be biased against algae that were hidden under the green algae canopy in summer or that were in crevices/under rocks. We also noted the presence of diverse heterotrophs such as anemones, sea sponges, small gobies, and shrimps. Calcifying invertebrates were represented by four gastropod species: *Phorcus lineatus*, *Patella ulyssiponensis*, *Patella vulgata* and *Gibbula pennanti*.

Study design and seawater manipulation

Fieldwork was conducted during the low-tide emersion periods, day and night. We refer to the period from the beginning to the end of the pool emersion as a "low-tide emersion period" and to each seasonal sampling period as a "field session" (**Table 1**). We sampled during three seasons: winter (February 2020 and 2021), spring (April 2021), and summer (September 2020 and 2021). During each field session, all the pools experienced both "future" (approximately year 2100 under high emissions) and present-day ("present", non-manipulated control) initial carbonate chemistry conditions. During each low-tide emersion period (n = 23), we randomly selected two or three pools in which we decreased pH to 7.5 at the start of the emersion. The following low-tide emersion period, this was reversed and pools that had been subject to present-day conditions in the previous low-tide emersion period were subject to future conditions and *vice versa*. However, due to diverse constraints, in two of the 23 emersion periods all the pools were left under present-day conditions.

Table 1: Sampling schedule: The dates of each field session are presented. Pools were monitored throughout multiple low-tide emersion periods (diurnal and nocturnal).

		Low-tide emersion periods (N)	
Season	Dates	Diurnal	Nocturnal
Winter	14-17 February 2020	2	0
	9-19 February 2021	8	2
Spring	28-29 April 2021	2	0
Summer	2-11 September 2020	5	1
	6-9 September 2021	0	3

In this experiment, we compared "present" and "future" seawater carbonate chemistry conditions. To simulate "future" carbonate chemistry conditions, we added small volumes of CO_2-enriched seawater (total of ~100-200 mL) at the start of the emersion period in 50 mL increments until the well-mixed pool water reached the desired pH levels (pH = 7.65, reached in less than 10 min.). CO_2-enriched seawater was prepared by super-saturating adjacent seawater in CO_2 using a high-pressure CO_2 cylinder.

Sampling and measurement of seawater parameters

Temperature, salinity, pH, oxygen, and ammonium: From the start of the emersion period, we measured five parameters periodically using HACH-Lange (Loveland, USA) probes: temperature, pH_T (IntelliCAL PHC101, accuracy: ± 0.02 pH units), salinity (conductivity probe IntelliCAL CDC401, ± 0.1 units), oxygen concentration (optical sensor IntelliCAL LDO101, accuracy: ± 0.1 mg L^{-1} for 0 to 8 mg L^{-1}, ± 0.2 mg L^{-1} for greater than 8 mg L^{-1}, maximum 22 mg L^{-1}) and NH_4^+ concentration (ion selective electrode IntelliCAL ISENH4181, range: 0.018 - 9000 mg L^{-1} NH_4^+-N). Pools were well-mixed before any measurement to assure no influence of gradients forming in the pools. The measurement frequency during the emersion periods was every 15-20 min during the day (n = 1392) and reduced to once an hour at night (n = 159), when temperature, pH and light variations were limited or absent. pH was calibrated on the total scale (pH_T) using TRIS (2-amino-2-hydroxy-1,3-propanediol) and AMP (2-aminopyridine) buffer solution with a salinity of 35.0, following the recommendations from (Dickson et al., 2007).

215   *Total alkalinity:* Discrete samples for total alkalinity (TA) analysis were collected hourly. The
216   average time between two samples was 1.0 ± 0.2 hours (n = 492, median = 1.0) during daytime
217   and 1.4 ± 0.9 hours (n = 135, median = 1.0) during nighttime. Seawater (150 mL) was filtered with
218   0.7 μm GF/F borosilicates filters directly after sampling. These samples were stored in a dark cool
219   box until the end of the tide (max. 7 h). Upon return to the lab, they were stored at 4°C in the dark
220   until they were either analyzed within the week or poisoned with 50 μL of saturated $HgCl_2$ (see
221   "*sample processing*"). TA was assessed potentiometrically using 50.0 ± 0.5 g of seawater and a
222   semi-automated titration system (0.1 M HCl, Titrino 848 plus by Metrohm, Switzerland; electrode
223   calibrated on the National Bureau of Standards scale). TA was determined using Gran titration
224   (Gran, 1952) according to the method of Haraldsson et al. (1997) and verified against reference
225   standards provided by A. Dickson (Scripps Institute of Oceanography, University of South
226   California, San Diego, United States). TA samples were analyzed with single (n= 312) or duplicate
227   (n = 320) measurements (the median of the standard deviation between duplicates was 1.05 μmol
228   kg^{-1}). TA was salinity-normalized before further calculations, to take into account possible dilution
229   from rain or concentration from evaporation.

230   To take into account the influence of the changes in nutrients (NO_3^-, NO_2^-, PO_4^{3-} and NH_4^+)
231   on the changes in TA (Gazeau et al., 2015), we sampled seawater for nutrients in winter (February
232   2020) and summer (September 2020). Samples were taken during the day at the start and end of
233   the emersion periods in the five pools. Around 60 mL of seawater was immediately filtered on 0.2
234   μm cellulose filters, stored in 125 mL polyethylene bottles in a cool dark box (max. 7h), and then
235   frozen at -20 °C until analysis. Nutrient concentrations were obtained using an AA3 auto-analyzer
236   (Seal Analytical) using the method from Aminot & Kérouel (2007). Changes in nutrient
237   concentrations were near-negligible contributions to TA changes throughout a low-tide emersion
238   period (< 6 μmol kg^{-1} i.e., $< 2\%$ of the observed change in TA, see full details in **Supp. Mat.**
239   **Nutrients**) and thus are ignored here.

240   *Light measurements:* Surface irradiance (photosynthetically active radiation, PAR) was
241   continuously recorded (every minute) during experiments at the field station, using a Li-Cor flat
242   quantum light sensor (LI-190R) and logger (LI-1500, LI-COR, Germany).

243   *Adjacent waters:* Temperature, salinity, pH and TA (n = 5) were similarly sampled and measured
244   at the sampling site during ebb tide, for the three seasons.

Carbonate chemistry calculations

The carbonate system parameters (e.g., pCO_2, DIC concentration, CO_3^{2-} concentration, and Ω_a, the aragonite saturation state) were calculated from the measurements of pH_T, TA, temperature and salinity using the *R* package *seacarb* (Gattuso et al., 2021) with the default dissociation constants recommended by Dickson et al. (2007), except for the low temperatures encountered in February 2021 where the refined constants of Sulpis et al. (2020) were used. When salinity decreased by more than 1.5 units per hour, data were excluded to avoid rain effects in the present study. When calculated DIC and Ω_a were negative, likely due to inaccuracies in the measurement and computation of the carbonate system, values were approximated to be 0 (7/627 values). The air-sea gas fluxes due to net diffusive transport were considered to be negligible in the pools (see detailed explanation the *interactive discussion*).

Biological activity calculations

The rates of Net Community Calcification (NCC; mmol $CaCO_3$ m^{-2} h^{-1}) and Net Community Production (NCP) or Community Respiration (CR; mmol O_2 m^{-2} h^{-1} or mmol C m^{-2} h^{-1}) were calculated between two consecutive sampling times. These rates respectively represent the measured changes of net $CaCO_3$ precipitation and net organic carbon production (or oxygen consumption) by the community. Positive NCC represents net $CaCO_3$ precipitation (gross precipitation > dissolution) and negative rates represent net dissolution (dissolution > precipitation). NCP is positive when the community primary production exceeds respiration and negative when community primary production is less than respiration. We use CR (not NCP) for nights, when there is no primary production (oxygen consumption and carbon release only).

NCC was calculated using the alkalinity anomaly method (Smith & Key, 1975). Briefly, for each mol of $CaCO_3$ precipitated, two moles of HCO_3^- combine with Ca^{2+}, and TA decreases by two moles (*Eq. 1*). Two independent estimates of NCP (or CR) were calculated, one derived from changes in ΔO_2 (NCP_{O2} or CR_{O2}) and one derived from ΔDIC and NCC (NCP_{DIC} or CR_{DIC}).

NCC and NCP (or CR) were thus calculated as follows:

$$\text{NCC} = \frac{\Delta TA}{2\Delta t} \times \frac{V}{S} \qquad (1)$$

$$NCP \ (or \ CR)_{O2} \ = \ \frac{\Delta O_2}{\Delta t} \times \frac{V}{S} \qquad (2)$$

$$NCP \ (or \ CR)_{DIC} \ = \ \frac{-\Delta DIC}{\Delta t} \times \frac{V}{S} - NCC \qquad (3)$$

with ΔTA (mmol L^{-1}), ΔDIC (mmol L^{-1}) and ΔO_2 (mmol L^{-1}) the change in concentration of TA, DIC and O_2, between consecutive samples and Δt the duration between consecutive samples (h), V pool volume (L), S the pool surface area (m^2).

Up to seven NCC and NCP (or CR) rates were calculated for each pool during each emersion period (one per hour). These rates were used to investigate the direct correlation between biological activity and environmental factors such as light intensity or Ω_a.

Rates calculated this way are however not independent from each other (i.e., the rate measured at t+2 is dependent on the rate at t+1), limiting further statistical analyses on the effect of the treatment. This is why, to investigate the effect of pH treatment ("present" vs. "future") on community biological activity, we also calculated NCC and NCP or CR using linear regressions (NCC_{lm} and NCP_{lm} or CR_{lm}) between TA, [DIC] and [O_2] and time after the start of the emersion period (for detailed results of the regressions, e.g., goodness-of-fit, see **Supp. Mat. LM1-3**). The few data from diurnal tides that were taken after sunset were excluded from these regressions. For oxygen, data ~~was~~were limited to the first three hours of emersion as high O_2 concentrations (>22 mg L^{-1}) and supersaturation (>200 %) led to inaccurate measurements and/or possible oxygen degassing afterwards (see **Supp. Mat. LM2**). This regression approach provides a single estimate of the rate of NCC, NCP_{DIC} (or CR_{DIC}) and NCP_{O2} (or CR_{O2}) for each pool during each emersion period (n = 17 diurnal and 6 nocturnal low-tide emersion periods x 5 pools = 115). These rates were then used in generalized linear mixed models (GLMM) to assess the effect of pH treatment on diurnal and nocturnal biological activity (see "*statistical analyses*" below).

We calculated community calcification and production budgets (respectively CCB and CPB) at emersion as an indication of the night/day balance in calcification and production: when CCB/CPB is positive the pool community calcifies/produces more by day than they dissolve/respire at night. Both were calculated for winter (February 2020 and 2021) and summer (September 2020 and 2021) for each pool as follows:

$$CCB \ = \ NCC_D + NCC_N \qquad (4)$$

$$\text{CPB} = NCP_D + CR_N \qquad\qquad (5)$$

with NCC_D and NCP_D (> 0) the average diurnal NCC and NCP for a given pool for a treatment and a season and NCC_N and CR_N (< 0) the average nocturnal NCC and dark respiration for the same conditions. Three approaches were used for estimating CPB, given the uncertainties of each NCP estimate (see discussion): (1) O_2-derived estimates of NCP (CPB_{O2}), (2) DIC- derived estimates (CPB_{DIC}) and (3) a "mixed" approach that combined nocturnal CR_{O2} and diurnal NCP_{DIC} (CPB_m), under the assumption that one mol of carbon is produced/consumed when one mol of O_2 is produced/consumed. Although CPB resemble gross community production in the way the rates are calculated (difference between light and dark net production/respiration rates), if one wanted to reuse these rates for gross community production, they should be do so with care due to differences in night and day temperature (see extended discussion on this subject in Bracken et al., 2022). The treatment effect was assessed on CCB and CPB by comparing the change due to the "future" treatment in each pool.

Statistical analyses

All data are presented as mean ± standard deviation (SD). The analyses were made using the software R (R Core Team, 2017). The level of significance used was 5%. Because data were measured on the same five pools but on different days for different treatments, we used GLMM to test for the effect of treatment on NCC_{lm} and on O_2 and DIC-derived NCP_{lm} (or CR_{lm}), assigning sampling days (i.e., low-tide emersion periods) as the random factor and pools (five levels), mean temperature of the pool during low-tide emersion period (a continuous proxy for season) and treatment (*Treat*: "future" vs. "present") as fixed factors. This was performed using the *R* package *nlme* (Pinheiro et al., 2018). Models with and without standardized residuals were compared using ANOVAs and, when different, Akaike Information Criteria (AIC) was used to choose the best fitted-model of the two. For GLMM, mean daily PAR was not used as it has strong collinearity with mean daily temperature/season. We used ANOVAs to test the effect of temperature, pool and treatment on initial (averaged over the first hour of emersion) and final (averaged for > 5 hours after emersion) carbonate chemistry conditions. The normality of the data was tested using Shapiro–Wilk tests and qq-plots, while variance homogeneity was tested with Bartlett tests.

329

RESULTS

1/ Environmental conditions

Adjacent waters: Temperatures (and salinity) measured in the seawater adjacent to the pools were 6-7°C in winter (February; salinity S=35.0), 11-12°C in spring (April; S=35.5) and 17-18°C in summer (September; S=36.0). This seawater was characterized by average pH_T of 8.01 ± 0.06 units, total alkalinity of 2319 ± 6 μmol kg^{-1}, pCO_2 of 445 ± 69 μatm, $\Omega_a = 2.2 \pm 0.3$ and $[O_2] = 100 \pm 1$ % of air saturation (or 10.1 ± 1.5 mg L^{-1}; n=5).

Light duration and intensity: In Roscoff, day:night (i.e., no light) periods are typically 10h:14h in February, 14h:10h in April and September. Photosynthetically active radiation (PAR) was two to three times higher in spring/summer (**Fig. 3A**: April/September ~1500 μmol m^{-2} s^{-1}) than in winter (February ~500 μmol m^{-2} s^{-1}).

Carbonate chemistry conditions at the start of the emersion period (< 1h post emersion): Both for diurnal and nocturnal tides, the initial pH was significantly lower in pools with added CO_2 than in the present-day pools (Day: $pH_T = 8.2 \pm 0.1$ vs. 7.5 ± 0.2 units; Night: 8.0 ± 0.1 vs. 7.4 ± 0.1 units for "present" and "future" pools respectively; *Treat p* < 0.001; detailed results in **Fig. S2-3**, **Table S1-2**). This corresponds to pCO_2 of 260 ± 100 vs. 1900 ± 835 μatm (day) and 510 ± 90 vs. 2310 ± 410 μatm (night) for pools in "present" and "future" conditions respectively. Adding CO_2 in the pools increased the mean DIC concentration by 320 μmol kg^{-1} during the day and 240 μmol kg^{-1} during the night. In "present-day" conditions, the pools started at supersaturated levels with regards to aragonite (day: $\Omega_a = 3.3 \pm 1.3$, night: 2.2 ± 0.3). Adding CO_2 significantly decreased Ω_a (Treat: p < 0.001, **Table S1**) leading to initial "future" conditions often undersaturated with regards to aragonite ($\Omega_a = 0.8 \pm 0.5$) by day and always undersaturated conditions by night ($\Omega_a = 0.6 \pm 0.1$). Furthermore, in "future" diurnal conditions, pools were always undersaturated with respect to aragonite from the start of the emersion period in February ($\Omega_a = 0.5 \pm 0.2$) but not in April ($\Omega_a = 1.1 \pm 0.7$) and September ($\Omega_a = 1.2 \pm 0.5$; **Table S1**). At the start of emersion, total alkalinity was 2303 ± 34 μmol kg^{-1} (similar to adjacent seawater), and uncorrelated with treatment (p > 0.05) and temperature (p > 0.6).

357   As data was averaged on the first hour post-emersion, the mean initial oxygen concentration calculated was already affected by NCP by day (14.0 ± 2 mg O_2 L^{-1}) and CR by night (9.5 ± 1.5 mg O_2 L^{-1}; vs. 10.1 ± 1.5 mg O_2 L^{-1} for adjacent seawater). This was also visible in CO_2 partial pressure, with lower pCO_2 than expected during the first hour post-emersion by day (262 ± 102 µatm vs. 445 ± 69 µatm for adjacent seawater) and higher pCO_2 at night (508 ± 88 µatm) in the "present-day" conditions.

2/ Diurnal tides

Diurnal pool chemistry: Starting from the aforementioned values at emersion, the pools followed a clear temporal evolution due to solar irradiance and community metabolism (**Fig. 3**). Firstly, we observed increases in salinity (+1.5 units on average, **Fig. 3A**) and temperature (+4°C in September, +6°C in April on average) in summer and spring. In winter, temperatures tended to decrease (-1.7°C on average) with air temperatures colder than that of the seawater; salinity was stable (35.5 ± 0.8).

       Secondly, we observed positive NCP corroborated by a doubling in oxygen concentration (**Fig. 3A**) a few hours after the start of emersion. In parallel, the seawater DIC concentration decreased by half from the initial concentration (from 2130 ± 195 to 1140 ± 560 µmol kg^{-1}; **Fig. 3B**), the range of which largely depended on the season (**Fig. S2**). For instance, in February, DIC consumption in pool seawater averaged ~700 µmol kg^{-1} over a low-tide period, while it averaged ~1500 µmol kg^{-1} in September. Particularly extreme conditions, with DIC concentrations effectively reaching 0 µmol kg^{-1}, were observed in two of the pools, at three tides in September 2020 (see further details below in "*5/ The particular case of September 2020 tides*"). At the end of diurnal emersions, average pCO_2 was always below 100 µatm, reaching as low as 1 ± 2 µatm in September (**Fig. 3B**, **Table S1**). As a result, diurnal pH_T increased to 9.1 ± 0.6 by the end of emersion, with maximum values up to 10.3 in summer (**Fig. 3B**). At the end of a diurnal emersion period, the pools' pH was stable, reaching either a plateau or decreasing after sunset (see PAR in **Fig. 3A**). Similarly, at the end of diurnal emersion periods, Ω_a was high (5.6 ± 3.0 on average; max 10.4). Lastly, we observed a diurnal decrease in TA by 415 µmol kg^{-1} on average, indicative of net calcification.

385   It is noteworthy that the carbonate chemistry conditions experienced at the end of diurnal
386   emersion converged whatever the initial treatment (**Fig. S2**, **Table S1**). For instance, while Ω_a was
387   significantly different between treatments at the start of the emersion period, both treatments
388   reached similar Ω_a at the end of emersion (> 5 h) of around 5.3 ± 2.2 (ANOVA: Treat: $p = 0.1$,
389   Temp: $p = 0.002$, Pool: $p = 0.01$). There was less convergence for pH_T where, even five hours after
390   emersion, there were still statistically significant, albeit small, differences between treatments (p
391   < 0.001 for pH_T with 9.2 ± 0.6 for "present" and 9.0 ± 0.6 for "future" pools).

392   **Diurnal biological activity:** Net community production was positive during daytime, except at
393   sunset (**Fig. 3C**). NCP was significantly correlated to light intensity (PAR) and further results for
394   hourly NCP and their correlation to hourly averaged PAR, Ω_a and temperature can be found in the
395   **Supp. Mat.** (**Fig. ~~S5~~S6** and **~~S6~~S7**).

396   As expected, seasons/temperature affected net oxygen production (O_2-derived NCP_{lm}),
397   increasing from 7 ± 3 mmol O_2 m^{-2} hr^{-1} in February to 18 ± 11 mmol O_2 m^{-2} hr^{-1} in September
398   (**Fig. 4A** and **Table 2A**: GLMM, $p < 0.001$). CO_2 addition increased O_2-derived NCP_{lm} by 20~~%,~~
399   % on average over all seasons, from 10 ± 7 mmol O_2 m^{-2} hr^{-1} in "present" conditions to 12 ± 9
400   mmol O_2 m^{-2} hr^{-1} ($p = 0.0015$). Net oxygen production differed across pools ($p < 0.003$), with
401   significantly more productivity in pool C (17.6 ± 12.7 mmol O_2 m^{-2} hr^{-1}) and D (10.6 ± 5.6 mmol
402   O_2 m^{-2} hr^{-1}), compared to the pools A, B and E (8.1 ± 4.1 mmol O_2 m^{-2} hr^{-1}).

403   Results are similar for DIC-derived NCP_{lm} (**Fig. 4A** and **Table 2B**), with primary
404   production ranging from 6 ± 2 mmol C m^{-2} hr^{-1} in February up to 12 ± 5 mmol C m^{-2} hr^{-1} in
405   September ($p < 0.001$). As for O_2-derived NCP_{lm} CO_2 addition increased DIC-derived NCP_{lm} by
406   20 % on average over all seasons ($p < 0.001$, **Fig. 4A**). This increase was particularly apparent in
407   the summer, where NCP_{lm} increased from 11 ± 4 mmol m^{-2} hr^{-1} in the "present" treatment to $15 \pm$
408   5 mmol C m^{-2} hr^{-1} in the "future" treatment (+ 35 %). ~~Compared to pool A,~~
409   ~~productivity~~Productivity (NCP_{lm}) was significantly lower in pools B and E than in pool A, and
410   significantly higher in pools C and D ($p < 0.003$).

411   By day, with the exception of sunset, net community calcification was positive (NCC and
412    $NCC_{lm} > 0$: **Fig. 3C** and **4B**) and occurred in an environment that was supersaturated with regards
413   to aragonite (**Fig. 3B**). This was with the exception of a few emersion periods in September 2020

414   where dissolution was observed despite high saturation state conditions (further details below).

415   Similar to NCP_{lm}, diurnal net calcification rates (NCC_{lm}) were strongly influenced by

416   temperature/season (**Fig. 4B** and **Table 2C**: GLMM, $p < 0.001$) ranging from 1.2 ± 0.5 mmol

417     $CaCO_3$ m^{-2} hr^{-1} in February to 3.3 ± 1.3 mmol $CaCO_3$ m^{-2} hr^{-1} in September. NCC hourly rates

418   positively correlated with averaged Ω_a ($p < 0.0001$; NCC = 0.15 x Ω_a + 0.85; linear regression

419   presented in **Fig. ~~S6~~S7**), significantly but not strongly ($R^2 = 10\%$). CO_2 addition did not influence

420   NCC_{lm} rates during the day ($p = 0.47$). However, NCC_{lm} did differ across pools ($p < 0.003$): rates

421   were relatively low in pool E – lowest CCA cover (30%) – (1.4 ± 1.4 mmol $CaCO_3$ m^{-2} hr^{-1}), and

422   high in pool D – highest CCA cover (70%) – (2.2 ± 0.8 mmol $CaCO_3$ m^{-2} hr^{-1}) compared to the

423   three other pools (2.0 ± 1.25 mmol $CaCO_3$ m^{-2} hr^{-1}).

424   **Table 2:** **Results of the generalized linear mixed-effect models for A) O_2-derived NCP_{lm}**

425   **(mmol O_2 m^{-2} hr^{-1}), B) DIC-derived NCP_{lm} (mmol C m^{-2} hr^{-1}) and C) NCC_{lm} (mmol $CaCO_3$ m^{-2}**

426   **hr^{-1}) during the day and night**. The models include three fixed factors: *Temp* (mean temperature:

427   a continuous factor), *Treat* (for CO_2 "future" treatment vs. "present", two levels) and *pools* (vs. A,

428   five levels), and one random effect (*low-tide emersion period* or the calendar day at which the pool

429   was measured). Significant *p*-values are highlighted in bold.

430

A.	O$_2$-derived NCP$_{lm}$		Estimate	Standard Error	p-value
Day	**Intercept**		1.49	1.37	0.28
	Fixed Effects	*Temp*	0.54	0.13	**<0.001***
		Treat	1.09	0.33	**0.0015***
		Pools	A, B, E ≠ C, D		**<0.003***
	Random Effect	*Low-tide emersion period*	8.90	0.90	**<0.001***
Night	**Intercept**		2.87	0.98	**0.005***
	Fixed Effects	*Temp*	-0.43	0.06	**<0.001***
		Treat	-0.25	0.28	0.39
		Pools	A, B, D ≠ C, E		**<0.03***
	Random Effect	*Low-tide emersion period*	-3.46	0.87	**<0.001***

431

432

B.	DIC-derived NCP$_{lm}$		Estimate	Standard Error	*p*-value
Day	**Intercept**		2.3	1.08	**0.035***
	Fixed Effects	*Temp*	0.38	0.08	**<0.001***
		Treat	1.25	0.25	**<0.001***
		Pools	A ≠ B, C, D, E		**<0.003***
	Random Effect	*Low-tide emersion period*	7.7	0.7	**<0.001***
Night	**Intercept**		-0.94	1.4	0.51
	Fixed Effects	*Temp*	-0.92	0.19	0.053
		Treat	-0.25	0.28	**<0.001***
		Pools	A, B, D, E ≠ C		**0.016***
	Random Effect	*Low-tide emersion period*	1.61	0.57	**0.01***

433

C.	NCC$_{lm}$		Estimate	Standard Error	*p*-value
Day	**Intercept**		-0.16	0.31	0.61
	Fixed Effects	*Temp*	-0.13	0.02	**<0.001***
		Treat	0.06	0.08	0.47
		Pools	A, B, C ≠ D, E		**<0.003***
	Random Effect	*Low-tide emersion period*	-1.90	0.24	**<0.001***
Night	**Intercept**		0.64	0.26	**0.026***
	Fixed Effects	*Temp*	0.009	0.016	0.57
		Treat	0.28	0.07	**0.0017***
		Pools	A, B, C ≠ D, E		**<0.017***
	Random Effect	*Low-tide emersion period*	0.83	0.078	**<0.001***

434

3/ Nocturnal tides

Nocturnal pool chemistry: Seawater temperatures during the nights were stable (**Fig. 3A**) throughout the emersion period in summer (from $17.3 \pm 0.4°C$ < 1 h post-emersion to $17.2 \pm 0.2°C$ > 5 h post-emersion) and winter (from $8.4 \pm 1.4°C$ to $7.8 \pm 2.7°C$ in February; no April nights). We highlight the wide range of winter seawater temperatures with an exceptionally cold tidal cycle (5°C on the 13th of February 2021) due to air temperatures of 3-4°C (observations from the Île de Batz meteorological station). There was a decline in salinity at night in some winter emersion periods (**Fig. 3A**), due to high air humidity and/or rain. Data where salinity dropped by more than 1.5 units in less than an hour were removed from further analyses on net community calcification and respiration.

After five hours of emersion, O_2 concentration had decreased by half (from $\approx 10.1 \pm 1.5$ mg O_2 L^{-1} to 4.9 ± 3.3 mg O_2 L^{-1}) (**Fig. 3A**) due to community respiration. Simultaneously, pH_T decreased to 7.6 ± 0.2 ("present") or stayed at 7.4 ± 0.2 ("future"; **Fig. 3B and S2, Table S1**), with significant effects of pools, treatment and temperature ($p < 0.001$ for all three). DIC concentration increased by +256 µmol kg^{-1} on average over an emersion period. The range of this increase depended on the temperature and the pool: in winter (5-10°C), present-day pool seawater gained +130 µmol kg^{-1} (+60 for "future" pools) of DIC over an emersion period, when in summer they gained +370 µmol kg^{-1} for "present" ("future": +310 µmol kg^{-1}) pools. **(Fig. S3)**. Saturation state converged towards similar undersaturated levels at night (**Fig. 3B and S2**, **Table S1**): Ω_a stayed stable in the "future" treatment (0.7 ± 0.2 units on average) and decreased in the "present-day" treatment (-1.2 units from initial Ω_a). At the end of nocturnal emersion Ω_a were still statistically different due to the initial treatment ($p < 0.001$ for *Treat*, *Temp* and *Pools*).

Nocturnal biological activity: At night, oxygen was consumed, i.e., we observed dark respiration (CR; **Fig. 3C**). Community respiration (O_2-derived CR_{lm}) varied according to season (**Fig. 4A and Table 2A**: $p < 0.001$): temperature linearly increased nocturnal respiration rates from -1.0 ± 1.2 mmol O_2 m^{-2} hr^{-1} in February to -4.7 ± 1.3 mmol O_2 m^{-2} hr^{-1} in September. The CO_2 treatment did not influence night respiration ($p = 0.39$). Respiration rates were significantly influenced by pools ($p = 0.03$), probably linked to the relative biomass of heterotrophs and autotrophs; respiration was significantly higher in pool C (-4.6 ± 2.8 mmol O_2 m^{-2} hr^{-1}) and significantly lower in pool E (-2.4 ± 1.4 mmol O_2 m^{-2} hr^{-1}) than in pools A, B and D (-3.4 ± 2.1 mmol O_2 m^{-2} hr^{-1}).

465   Night respiration estimated using DIC and NCC was near zero ($CR_{lm} = -0.2 \pm 0.7$ mmol m^{-2} hr^{-1}). At these low rates, uncertainties associated with much higher rates of net dissolution

466   (negative NCC) sometimes led to spuriously positive DIC-derived CR estimates, hindering

467   interpretation. Nevertheless, DIC-derived community respiration was ten times lower in February

468   than in September (-0.2 $\pm$ 0.7 and -2.3 $\pm$ 1.1 mmol C m^{-2} hr^{-1} respectively), although it was not

469   than in September (-0.2 $\pm$ 0.7 and -2.3 $\pm$ 1.1 mmol C m^{-2} hr^{-1} respectively), although it was not

470   linearly driven by temperature ($p = 0.053$; **Fig. 4B** and **Table 2B**). Adding CO_2 to the pools

471   influenced DIC-derived community respiration in a way that was inverse to that seen with O_2, but

472   as stated above, this was likely an artifact of subtracting NCC from small DIC changes. As for O_2,

473   DIC-derived CR_{lm} significantly changed depending on the pools.

474   At night, the pools experienced significant net community dissolution (NCC < 0: **Fig. 3C**)

475   even when waters were supersaturated with regards to aragonite in the "present" treatment (**Fig.**

476   **3B**: $\Omega_a > 1$). Nocturnal net dissolution rates (NCC_{lm}) were not significantly affected by temperature

477   in the range investigated (5-18°C; **Fig. 4C** and **Table 2C**: $p = 0.57$). However, adding CO_2 in the

478   pools increased net dissolution rates ($p = 0.0017$) from -0.7 $\pm$ 0.3 mmol CaCO$_3$ m^{-2} hr^{-1} to -1.0 $\pm$

479   0.4 mmol CaCO$_3$ m^{-2} hr^{-1} (+40 %). Similarly, looking instead at hourly rates (NCC), dissolution

480   correlated significantly ($p < 0.0001$) with Ω_a (NCC = 0.34 x Ω_a – 1.22; $R^2 = 11$ %; **Fig. ~~S6~~S7**).

481   The strength of this correlation depended on seasons and pools (**Fig. ~~S7~~S8**). Net dissolution rates

482   (NCC_{lm}) significantly differed by pool ($p < 0.0017$): the lowest rates were observed in pool E (-

483   0.4 $\pm$ 0.2 mmol CaCO$_3$ m^{-2} hr^{-1}) – the pool with the lowest CCA cover –, and the highest dissolution

484   in pool D – the pool with the highest CCA cover (-1.0 $\pm$ 0.4 vs. -0.9 $\pm$ 0.3 mmol CaCO$_3$ m^{-2} hr^{-1}

485   for A, B and C).

486

487   **4/ Influence of the treatment on CPB and CCB**

488   Pools fixed more carbon during the day than they respired at night, i.e., the community production

489   budget (CPB: balance between night and day) was positive in all the pools, both in winter and

490   summer and whatever the treatment (**Fig. 5**). CPB$_{DIC}$ and CPB$_m$ estimates were typically lower

491   than CPB$_{O2}$ (in 14/20 cases and 18/20 cases respectively). The production budget was significantly

492   lower in winter than in summer (FEB: CPB$_{O2}$ = 3 $\pm$ 1 mmol O$_2$ m^{-2} h^{-1}, SEP: 7 $\pm$ 5 mmol O$_2$ m^{-2}

493   h^{-1}; t-test: t = -2.4, df = 9.8, $p = 0.03$). Adding CO_2 increased CPB in all the pools in summer by +

494   3.0 $\pm$ 2.1 mmol O$_2$ m^{-2} h^{-1}, an increase in production by 50 to 80 % (ΔCPB; **Fig. 5**). In winter, there

was no evidence of such a "fertilization effect" across the most accurate CPB estimates for this season (CPB_{O2}, CPB_m): we only observed a significant increase in production due to CO_2 addition in two of the pools (+60 % to +120 % for A and B). For the three other pools, CPB either induced minimal changes (< 20 % for C and E) or a decrease in production (D: down to -34 %). DIC-derived ΔCPB in winter (all positive) should be interpreted with caution since some nocturnal CR_{lm} were spuriously positive in the "future" treatment (see "*nocturnal biological activity*" above).

The pools calcified more during the day than they dissolved at night (CCB > 0), both in summer and winter (**Fig. 5**). CCB was significantly lower in winter than in summer (FEB: CCB = 0.2 ± 0.2 mmol $CaCO_3$ m^{-2} h^{-1}, SEP: 1.2 ± 0.6 mmol $CaCO_3$ m^{-2} h^{-1}; t-test: t = -5.2, df = 11.7, *p* = 0.0002). In winter, adding CO_2 decreased CCB by more than 80 % in pools C, D, and E (**Fig. 5**). The CO_2 addition even resulted in a transition from a positive community calcification balance to dissolution in pool C (133 % change, from +0.5 to -0.2 mmol $CaCO_3$ m^{-2} h^{-1}). For the two other pools (A and B), winter CO_2 addition increased their relatively small calcification balance (A: +87 %, from 0.1 to 0.2 mmol $CaCO_3$ m^{-2} h^{-1} and B: +71 %, from 0.2 to 0.3 mmol $CaCO_3$ m^{-2} h^{-1}). In summer, changes in CCB due to treatment appeared minimal in pools A, B and E (< 15 % change) and either increased (C: +67%) or decreased (D: -57%) in the two other pools. In analyses not presented here, when this budget takes into account winter night:day duration (14:10), all the pools' budgets switch to net dissolution in future conditions.

5/ The particular case of September 2020 tides

During diurnal tides of September 2020 (high PAR and high temperature summer conditions), we observed an unexpected phenomenon: dissolution occurred at extremely high pH_T values (9-10) in pools C and E (**Fig. 6**). Under these conditions effectively all the seawater DIC in these pools was consumed by photosynthesis and calcification (DIC ≈ 0 mmol kg^{-1}) four hours after emersion. As such, the CO_3^{2-} concentration was also effectively zero and the pools reached very low saturations states ($\Omega_a \approx 0$) despite high pH (**Fig. 6**). These conditions were quickly followed by indicators of $CaCO_3$ dissolution (increasing TA and DIC) instead of the expected diurnal precipitation. It is therefore noteworthy that dissolution may happen at high pH, and that pH and

523 Ω can decorrelate (**Fig. 7**) in situations with high photosynthesis and limited mixing of water
524 masses.

525

526 **DISCUSSION**

527 Temperate tidal pools are environments of extreme variability. In our pools, we observed seawater
528 temperatures that could increase by up to 10°C in a few hours compared to the adjacent ocean.
529 During diurnal emersion periods, oxygen concentrations doubled and pH could increase to pH 10
530 in present-day summer conditions. At night, pH routinely reached levels usually used as the
531 "treatment" for ocean acidification perturbation experiments (~7.6). Organisms present in the tidal
532 pools may therefore already be adapted or acclimatized to extreme variability in pH and saturation
533 state, which could affect their responses to ocean acidification (Andersson et al., 2015). For
534 example, CCA from a site with naturally high pCO_2 variability calcified ~50 % more than
535 individuals from a nearby site of low variability when submitted to oscillating high pCO_2
536 treatments (Johnson et al., 2014). Here we show that, even in intertidal communities likely already
537 acclimated or adapted to variable conditions, with potentially large phenotypic plasticity,
538 acidification can still modify net community production and calcification rates.

539 **Diurnal fertilization under CO₂ addition**
540 Adding CO_2 to simulate future seawater acidification in the pools led to a diurnal fertilization
541 effect. ~~This increase in the~~The community's net primary production increased by 20% on average
542 across all seasons, which was particularly visible in summer (+ 35%), ~~at higher~~when
543 temperatures/metabolic rates were high. Adding CO_2, we also added substrate for photosynthesis
544 in the form of DIC (**Fig. 3B**) that the algae of the pools can assimilate, potentially supporting
545 higher DIC use and algal primary production. This effect was apparent from the start of the
546 emersion, suggesting a direct effect of increasing DIC concentration in the pools. It seems that
547 photosynthesis in the pools was carbon-limited and that carbon addition therefore enhanced
548 primary production, in winter and to an even greater extent in summer. During photosynthesis, the
549 uptake of inorganic carbon leads to a significant decrease in DIC - even in present-day conditions.
550 Intertidal algae are typically adapted to this with coralline algae in particular containing CCMs
551 (CO_2 concentrating mechanisms) that allow them to achieve primary production in low DIC

552 concentrations (Raven, 2011). Increasing seawater DIC may however promote an increase in
553 active and/or passive CO_2 and HCO_3^- fluxes towards photosynthetic compartments. Borowitzka
554 (1981) found that the photosynthetic rate of an intertidal CCA was highest at pH 6.5 to 7.5
555 (increased from pH 8.1), a change in pH that was achieved using HCl, suggesting that increased
556 photosynthetic activity could also be linked to proton gradients/pumps and/or decreased energy
557 expenditure needed to operate CCMs rather than directly related to CO_2 gradients or higher
558 substrate availability.

559   In winter and summer, pools in present-day and future conditions were autotrophic at
560 emersion ($NCP_D > CR_N$, **Fig. 5**). If we consider the CPB as integrated diurnal NCP and nocturnal
561 CR over 24 hours (assuming equal day:night duration), this means that the pools always fixed
562 more carbon during the day than they respired at night at emersion ($NCP \gg CR$), regardless of
563 treatment. One methodological uncertainty we highlight regarding net production is that diurnal
564 DIC-derived NCP estimations were 50 % higher than O_2-derived NCP estimates (**Fig. 3C and Fig.**
565 **4**, $NCP_{DIC} = 1.6 \pm 0.05\ NCP_{O2}$ by day; $R^2 = 75$ %). This discrepancy was far less apparent during
566 nights, when methods agreed on respiration rates ($CR_{DIC} = 1.0 \pm 0.09\ CR_{O2}$; $R^2 = 56$ %). While
567 O_2-derived NCP appears accurate during the night, O_2 production during the day is likely to have
568 been underestimated due to degassing (e.g., visible formation of oxygen bubbles at the surface of
569 algae, >150 % air saturation by day vs. < 100 % at night). Thus, estimating diurnal net production
570 using oxygen measurements may not be appropriate in algae-dominated environments such as
571 these tidal pools. Nevertheless, despite the difference in absolute NCP estimates, both approaches
572 indicate a diurnal fertilization effect.

573

574 **Nocturnal dissolution under CO_2 addition**
575 In the present study, natural mesocosms - temperate coralline-dominated tidal pools - were used
576 to investigate the effect of ocean acidification on net calcification at the community level. As we
577 observed a fertilization effect of CO_2 addition by day, we could have expected that it would also
578 enhance diurnal calcification – as photosynthesis and calcification are tightly linked (Martin et al.,
579 2013; Martin et al., 2013; Williamson et al., 2017) -, but this was not observed. Treatment had no
580 significant effect on the daytime net calcification rates, and diurnal variability in calcification
581 appears to be predominately driven by PAR, temperature, and metabolic activity (NCP). Increasing
582 metabolic rates - in turn increasing calcification rates - may have however counterbalanced any

583   calcification suppression or increased dissolution due to acidification, making its effect invisible.

584   Noisette et al. (2013) similarly found no effect of pCO$_2$ treatment on light calcification for *E.*

585   *elongata*. However, the authors reported a significant decrease in light calcification in *L.*

586   *incrustans*, net calcification even switched to net dissolution in 750 and 1000 μatm pCO$_2$

587   treatments. While our "future" treatments started at pCO$_2$ levels higher than 1000 μatm, the fact

588   that CO$_2$ addition did not influence diurnal calcification could also be due to favorable saturation

589   state conditions in the micro-environment in which calcification occurs. The diffusive boundary

590   layer (DBL) can enhance CaCO$_3$ precipitation micro-environment conditions due to the uptake of

591   CO$_2$/DIC for photosynthesis. For instance, in light conditions, CCA surface pH has been shown to

592   reach as high as 8.6 (Houlihan et al., 2020) in surrounding seawater at pH 7.7 (+1.1 pH units),

593   which would be highly favorable to calcification. Although there are conflicting results indicating

594   that saturation state of the ambient seawater is a key driver of coralline algal calcification, the

595   biomineralization process in coralline algae has also been shown to present a certain degree of

596   biological control (de Carvalho et al., 2017; Nash et al., 2019). Recent work using boron isotopes

597   (δ11B) as a proxy for pH showed that coralline algae have ability to elevate pH at their site of

598   calcification (Cornwall et al., 2017). But more complex interactions may also be at work, e.g.,

599   CCA may use increases in HCO$_3^-$ (due to CO$_2$ dissolution) to calcify, making them more resistant

600   to ocean acidification, as suggested by Comeau et al. (2013).

601   There was net CaCO$_3$ dissolution in the pools at night (-0.7 mmol CaCO$_3$ m^{-2} hr^{-1}), even

602   when waters were still supersaturated with regards to aragonite under present-day conditions.

603   Night dissolution may be a sign that the DBL of the calcifiers inhabiting the pools is

604   undersaturated, possibly as a result of respiration. Indeed, Houlihan et al. (2020) observed that

605   nocturnal algal respiration by CCA, increased CO$_2$ in the DBL, decreasing pH of the DBL by 0.1

606   units. Such a small pH decrease is however unlikely to explain alone an undersaturation of the

607   calcifying environment as aragonite saturation state was still above 1.2 in most of the "present-

608   day" conditions. However, given the solubility of high-Mg calcite - the mineral composing *L.*

609   *incrustans* and *E. elongata* in particular (Ries, 2011) - can be twice that of aragonite (Sulpis et al.,

610   2021; Yamamoto et al., 2012), it is possible that undersaturation already occurs at night for this

611   mineral even for $\Omega_a > 1$. Another reason for night dissolution might be linked to the patellid limpet,

612   an opportunistic (Schaal & Grall, 2015) and dominant grazer in rockpools, that can be particularly

613   active at night(Lorenzen, 2007). Encrusting coralline algae can be an important food source for

these herbivores and the large percentage of grazed coralline algal $CaCO_3$ in their gut (Maneveldt et al., 2006) could dissolve easily at night.

Adding CO_2 (from 445 to 1500-2000 µatm) at the start of emersion significantly increased net dissolution (NCC_{lm}), by 40 % in summer and 70 % in winter. In a previous single-species experiment, Noisette et al. (2013) demonstrated that - for *L. incrustans* from an area close to our site – dark dissolution doubled with increasing pCO_2 (1000 µatm vs. 380 µatm), unlike *E. elongata*, for which there was no effect of pCO_2: the ACA even calcified in the dark up to 750 µatm (see also similar results from Egilsdottir et al., 2013). Since *L. incrustans* is the major calcifying species of the tidal pools we studied, it is likely this species drives the results we observed at the pool community scale. Regardless of the treatment, nocturnal net dissolution rates (NCC) were also significantly correlated with Ω_a, results similar to those found by Kwiatkowski et al. (2016) in temperate tidal pools of California, without CO_2 addition.

In summer, pools in present-day and future conditions were precipitative (CCB > 0), meaning that diurnal net calcification exceeded nocturnal net dissolution, regardless of treatment. Adding CO_2 in summer did not consistently change CCB, with most pools showing little change in CCB due to treatment. By contrast, in the colder winter, the calcification budget was at least 50 % lower than in summer ("present"), with some pools that had comparable net calcification during the day to net dissolution at night. During this season, adding CO_2 had variable impacts on CCB, decreasing it in three of the pools by more than 80 % and increasing relatively small CCB in two. These variable effects may be due to differences in community composition and highlight the difficulty in generalizing the results of natural mesocosm manipulations in which the initial community composition is not controlled. Nevertheless, we expected CO_2 addition to have a greater negative effect in winter (more dissolution) than in summer, with saturation states being lower due to colder temperatures, making it more of a "crucial"/ "bottleneck" season. This emphasizes the need to study the effect of ocean acidification across seasons and temperature ranges, especially given the associated changes in algal community composition and metabolic activity.

A limit of the CCB in the current study is that we only considered the tidal pools as closed (emersed) systems. However, in an acidifying ocean, tidal pool communities are submersed for nearly 12 hours per day, resulting in long exposure to low pH. More accurate and realistic budgets would need to integrate these

644 immersion periods, which might have additive negative effects on calcification (see e.g., Legrand et al.,
645 2018 for tidal assemblage experiments on net production/respiration).
646
647 **Instances of aragonite undersaturation at high pH**
648 An unexpected phenomenon happened in the pools C and E in summer: although we measured
649 very high pH values, we observed that total alkalinity suddenly increased, a sign of fast net
650 dissolution. When we then computed the carbonate chemistry, the saturation states were
651 surprisingly low ($\Omega_a = 0$ for $pH_T = 10$), which was due to near-zero DIC concentrations – and thus
652 near-zero CO_3^{2-} concentrations. In these particular conditions, which occurred towards the end of
653 the tidal emersion period, any $CaCO_3$ precipitation was less than dissolution; precipitation may
654 even have been impossible due to a lack of DIC substrate. In intertidal pools with a high density
655 of *Zostera marina*, Miller & Kelley (2021) observed a similar decoupling between pH and Ω_a with
656 increases in pH not leading to an increase in saturation state at high pH values due to a lack of
657 DIC/CO_3^{2-}. In our study, we observed even more drastic decoupling between expected changes in
658 pH, Ω_a and NCC, with some of the fastest net dissolution rates observed at very high pH and very
659 low Ω_a values that were a consequence of near complete consumption of DIC by community
660 production (**Fig. 7**). Macroalgae cultivation has been proposed as a method of bioremediation to
661 local acidification, in particular to improve aquaculture environments (e.g., Bergstrom et al., 2019;
662 Gao & Beardall, 2022): increase in algal or marine plant cover would reverse or buffer the negative
663 effects of acidification on heterotroph calcifiers. Our results and those of Miller & Kelley (2021)
664 suggest that phytoremediation should not consider pH as the sole indicator for "acidification
665 remediation", and that periodical decreases in saturation state in macroalgae- or seaweed-
666 dominated environments in summer (and during marine heatwaves), may need to be considered
667 for these proposed types of remediations.
668
669 **Conclusion**
670 Relative to its area, human societies are disproportionately reliant on the coastal ocean for the
671 provision of natural resources and climate regulation. Yet our understanding of how anthropogenic
672 carbon emissions and associated ocean acidification will influence natural coastal ecosystems and
673 community metabolism remains limited. In the present study, we manipulated the carbonate
674 chemistry of natural temperate intertidal pools to explore the potential impact of future ocean

acidification on community-level calcification and production. We find evidence of large seasonal, diel and community-specific differences in the sensitivity of intertidal community metabolism to acidification. Diurnally, acidification was found to enhance net community production, with this "fertilization effect" indicating algal photosynthesis is naturally carbon limited in such environments at emersion. Diurnal net community calcification was unaffected by acidification. In contrast, nocturnal acidification resulted in greater net community dissolution in the intertidal pools yet had no consistent effect on community respiration. Integrated over day/night emersion periods, the intertidal mesocosms maintained positive net community calcification and production under both present-day and future conditions. Albeit considerable differences between individual pools and strong seasonal dependencies, our results indicate that the net calcification and production of temperate intertidal communities - likely acclimated/adapted to variable conditions - could be affected by future acidification.

ACKNOWLEDGEMENTS

We thank Elsa Perruchini, Léonard Dupont, Corentin Clerc, Priscilla Le Mezo, Alban Planchat, Maud Chevalier, Anne Cornillon, Annabel Antheaume, Maïlys Roux and Clarisse Dufaux for their kind assistance with fieldwork. This project is fully funded by the CHANEL research chair: *Understanding the Linkages between the Ocean, the Carbon Cycle, and Marine Ecosystems under Climate Change*. Data presented for adjacent Atlantic waters characteristics (main text and the supplementary material) were kindly provided by the SOMLIT network database (Service d'Observation en Milieu Littoral; www.somlit.fr) on June 2022.

AUTHORS CONTRIBUTIONS

ND, SM and LK designed the experiments and ND carried them out with help from all co-authors. ND analysed the data and prepared the manuscript, with contributions from all co-authors.

COMPETING INTERESTS

The authors declare that they have no conflict of interest.

DATA AVAILABILITY

705   Raw data and linear regression model results are provided as supplementary in the Appendix.

706

BIBLIOGRAPHY:

Albright, R., Caldeira, L., Hosfelt, J., Kwiatkowski, L., Maclaren, J. K., Mason, B. M., Nebuchina, Y.,
Ninokawa, A., Pongratz, J., Ricke, K. L., Rivlin, T., Schneider, K., Sesboüé, M., Shamberger, K.,
Silverman, J., Wolfe, K., Zhu, K., & Caldeira, K. (2016). Reversal of ocean acidification enhances
net coral reef calcification. *Nature*, *531*(7594), Article 7594.
https://doi.org/10.1038/nature17155

Albright, R., Takeshita, Y., Koweek, D. A., Ninokawa, A., Wolfe, K., Rivlin, T., Nebuchina, Y., Young, J., &
Caldeira, K. (2018). Carbon dioxide addition to coral reef waters suppresses net community
calcification. *Nature*, *555*(7697), Article 7697. https://doi.org/10.1038/nature25968

Aminot, A., & Kérouel, R. (2007). *Dosage automatique des nutriments dans les eaux marines : Méthodes
en flux continu*. Editions Quae.

Andersson, A. J., Kline, D. I., Edmunds, P. J., Archer, S. D., Bednaršek, N., Carpenter, R. C., Chadsey, M.,
Goldstein, P., Grottoli, A. G., Hurst, T. P., King, A. L., Kübler, J. E., Kuffner, I. B., Mackey, K. R. M.,
Menge, B. A., Paytan, A., Riebesell, U., Schnetzer, A., Warner, M. E., & Zimmerman, R. C. (2015).
Understanding ocean acidification impacts on organismal to ecological scales. *Oceanography*,
28(2), 16–27.

Barry, J., Hall-Spencer, J., & Tyrrell, T. (2010). In situ perturbation experiments: Natural venting sites,
spatial/temporal gradients in ocean pH, manipulative in situ pCO$_2$ perturbations. In *Guide to best
practices in ocean acidification research and data reporting* (pp. 123–136).

Bergstrom, E., Silva, J., Martins, C., & Horta, P. (2019). Seagrass can mitigate negative ocean acidification
effects on calcifying algae. *Scientific Reports*, *9*(1), Article 1. https://doi.org/10.1038/s41598-
018-35670-3

729 Borowitzka, M. A. (1981). Photosynthesis and calcification in the articulated coralline red algae

730   *Amphiroa anceps* and *A. foliacea*. *Marine Biology*, *62*(1), 17–23.

731   https://doi.org/10.1007/BF00396947

732 Bracken, M. E. S., Miller, L. P., Mastroni, S. E., Lira, S. M., & Sorte, C. J. B. (2022). Accounting for variation

733   in temperature and oxygen availability when quantifying marine ecosystem metabolism.

734   *Scientific Reports*, *12:825*, Article 1. https://doi.org/10.1038/s41598-021-04685-8

735 Cocquempot, L., Delacourt, C., Paillet, J., Riou, P., Aucan, J., Castelle, B., Charria, G., Claudet, J., Conan,

736   P., Coppola, L., Hocdé, R., Planes, S., Raimbault, P., Savoye, N., Testut, L., & Vuillemin, R. (2019).

737   Coastal ocean and nearshore observation: A French case study. *Frontiers in Marine Science*, *6*.

738   https://doi.org/10.3389/fmars.2019.00324

739 Comeau, S., Carpenter, R. C., & Edmunds, P. J. (2013). Coral reef calcifiers buffer their response to ocean

740   acidification using both bicarbonate and carbonate. *Proceedings of the Royal Society B:*

741   *Biological Sciences*, *280*(1753), 20122374. https://doi.org/10.1098/rspb.2012.2374

742 Cornwall, C. E., Comeau, S., & McCulloch, M. T. (2017). Coralline algae elevate pH at the site of

743   calcification under ocean acidification. *Global Change Biology*, *23*(10), 4245–4256.

744   https://doi.org/10.1111/gcb.13673

745 Cox, T. E., Schenone, S., Delille, J., Díaz-Castañeda, V., Alliouane, S., Gattuso, J.-P., & Gazeau, F. (2015).

746   Effects of ocean acidification on *Posidonia oceanica* epiphytic community and shoot

747   productivity. *Journal of Ecology*, *103*(6), 1594–1609. https://doi.org/10.1111/1365-2745.12477

748 de Carvalho, R. T., Salgado, L. T., Amado Filho, G. M., Leal, R. N., Werckmann, J., Rossi, A. L., Campos, A.

749   P. C., Karez, C. S., & Farina, M. (2017). Biomineralization of calcium carbonate in the cell wall of

750   Lithothamnion crispatum (Hapalidiales, Rhodophyta): Correlation between the organic matrix

751   and the mineral phase. *Journal of Phycology*, *53*(3), 642–651. https://doi.org/10.1111/jpy.12526

752   Dickson, A., Sabine, C. L., & Christian, J. R. (2007). *Guide to best practices for ocean CO$_2$ measurements*.

753   PICES Special Publication 3; 191 pp.

754   Dorey, N., Lançon, P., Thorndyke, M., & Dupont, S. (2013). Assessing physiological tipping point of sea

755   urchin larvae exposed to a broad range of pH. *Global Change Biology*, *19*(11), 3355–3367.

756   https://doi.org/10.1111/gcb.12276

757   Egilsdottir, H., Noisette, F., Noël, L. M.-L. J., Olafsson, J., & Martin, S. (2013). Effects of *p*CO$_2$ on

758   physiology and skeletal mineralogy in a tidal pool coralline alga *Corallina elongata*. *Marine*

759   *Biology*, *160*(8), 2103–2112. https://doi.org/10.1007/s00227-012-2090-7

760   Foo, S., Byrne, M., Ricevuto, E., & Gambi, M. C. (2018). The carbon dioxide vents of Ischia, Italy, a natural

761   system to assess impacts of ocean acidification on marine ecosystems: An overview of research

762   and comparisons with other vent systems. *Oceanography and Marine Biology: An Annual*

763   *Review*, *56*, 237–310. https://doi.org/10.1201/9780429454455-4

764   Ganning, B. (1971). Studies on chemical, physical and biological conditions in swedish rockpool

765   ecosystems. *Ophelia*, *9*(1), 51–105. https://doi.org/10.1080/00785326.1971.10430090

766   Gao, K., & Beardall, J. (2022). Using macroalgae to address UN Sustainable Development goals through

767   CO$_2$ remediation and improvement of the aquaculture environment. *Applied Phycology*, *3*(1),

768   360–367. https://doi.org/10.1080/26388081.2022.2025617

769   Gattuso, J.-P., Epitalon, J.-M., Lavigne, H., & Orr, J. (2021). *seacarb: Seawater carbonate chemistry with*

770   *R. R package version 3.2.16 http://CRAN.R-project.org/package=seacarb*.

771   Gazeau, F., Urbini, L., Cox, T., Alliouane, S., & Gattuso, J. (2015). Comparison of the alkalinity and calcium

772   anomaly techniques to estimate rates of net calcification. *Marine Ecology Progress Series*, *527*,

773   1–12. https://doi.org/10.3354/meps11287

774   Gran, G. (1952). Determination of the equivalence point in potentiometric titrations. Part II. *The Analyst*,

775   *77*(920), 661. https://doi.org/10.1039/an9527700661

776   Haraldsson, C., Anderson, L. G., Hassellöv, M., Hulth, S., & Olsson, K. (1997). Rapid, high-precision

777   potentiometric titration of alkalinity in ocean and sediment pore waters. *Deep Sea Research Part*

778   *I: Oceanographic Research Papers*, *44*(12), 2031–2044. https://doi.org/10.1016/S0967-

779   0637(97)00088-5

780   Houlihan, E. P., Espinel-Velasco, N., Cornwall, C. E., Pilditch, C. A., & Lamare, M. D. (2020). Diffusive

781   boundary layers and ocean acidification: Implications for sea urchin settlement and growth.

782   *Frontiers in Marine Science*, *7*. https://www.frontiersin.org/articles/10.3389/fmars.2020.577562

783   Hurd, C. L., Beardall, J., Comeau, S., Cornwall, C. E., Havenhand, J. N., Munday, P. L., Parker, L. M., Raven,

784   J. A., McGraw, C. M., Hurd, C. L., Beardall, J., Comeau, S., Cornwall, C. E., Havenhand, J. N.,

785   Munday, P. L., Parker, L. M., Raven, J. A., & McGraw, C. M. (2019). Ocean acidification as a

786   multiple driver: How interactions between changing seawater carbonate parameters affect

787   marine life. *Marine and Freshwater Research*, *71*(3), 263–274.

788   https://doi.org/10.1071/MF19267

789   IPCC. (2019). *IPCC Special Report on the Ocean and Cryosphere in a Changing Climate* (H. O. Pörtner, D.

790   Roberts, V. Masson-Delmotte, & P. Zhai, Eds.). Cambridge University Press, UK.

791   https://doi.org/10.1017/9781009157964

792   Jia, G., E. Shevliakova, P. Artaxo, N. De Noblet-Ducoudré, R. Houghton, J. House, K. Kitajima, C. Lennard,

793   A. Popp, A. Sirin, R. Sukumar, & L. Verchot. (2019). Land–climate interactions. In *Climate Change*

794   *and Land: An IPCC special report on climate change, desertification, land degradation,*

795   *sustainable land management, food security, and greenhouse gas fluxes in terrestrial ecosystems*

796   (P.R. Shukla, J. Skea, E. Calvo Buendia, V. Masson-Delmotte, H.-O. Pörtner, D.C. Roberts, P. Zhai,

797   R. Slade, S. Connors, R. van Diemen, M. Ferrat, E. Haughey, S. Luz, S. Neogi, M. Pathak, J.

798   Petzold, J. Portugal Pereira, P. Vyas, E. Huntley, K. Kissick, M. Belkacemi, J. Malley).

799   https://www.ipcc.ch/srccl/chapter/chapter-2/

800 Johnson, M. D., Moriarty, V. W., & Carpenter, R. C. (2014). Acclimatization of the Crustose Coralline Alga

801   Porolithon onkodes to Variable pCO2. *PLOS ONE*, *9*(2), e87678.

802   https://doi.org/10.1371/journal.pone.0087678

803 Kottmeier, D. M., Chrachri, A., Langer, G., Helliwell, K. E., Wheeler, G. L., & Brownlee, C. (2022). Reduced

804   H+ channel activity disrupts pH homeostasis and calcification in coccolithophores at low ocean

805   pH. *Proceedings of the National Academy of Sciences*, *119*(19), e2118009119.

806   https://doi.org/10.1073/pnas.2118009119

807 Kroeker, K. J., Micheli, F., & Gambi, M. C. (2012). Ocean acidification causes ecosystem shifts via altered

808   competitive interactions. *Nature Climate Change*, *3*(2), 156–159.

809   https://doi.org/10.1038/nclimate1680

810 Kwiatkowski, L., Gaylord, B., Hill, T., Hosfelt, J., Kroeker, K. J., Nebuchina, Y., Ninokawa, A., Russell, A. D.,

811   Rivest, E. B., Sesboüé, M., & Caldeira, K. (2016). Nighttime dissolution in a temperate coastal

812   ocean ecosystem increases under acidification. *Scientific Reports*, *6*(1), Article 1.

813   https://doi.org/10.1038/srep22984

814 Kwiatkowski, L., Torres, O., Bopp, L., Aumont, O., Chamberlain, M., Christian, J. R., Dunne, J. P., Gehlen,

815   M., Ilyina, T., John, J. G., Lenton, A., Li, H., Lovenduski, N. S., Orr, J. C., Palmieri, J., Santana-

816   Falcón, Y., Schwinger, J., Séférian, R., Stock, C. A., … Ziehn, T. (2020). Twenty-first century ocean

817   warming, acidification, deoxygenation, and upper-ocean nutrient and primary production

818   decline from CMIP6 model projections. *Biogeosciences*, *17*(13), 3439–3470.

819   https://doi.org/10.5194/bg-17-3439-2020

820 Legrand, E., Riera, P., ~~Lutier, M~~Bohner, O., Coudret, J., ~~Grall, J.,~~ Schlicklin, F., Derrien, M., & Martin, S.

821   ~~(2019). Grazers increase the sensitivity~~(2018). Impact of ~~coralline algae to~~ ocean acidification

822   and warming. ~~*Journal*~~ on the productivity of ~~*Sea*~~a rock pool community. *Marine Environmental*

Research, ~~148–149~~, ~~1–7~~*136*, 78–88.

https://doi.org/10.1016/j.~~seares.2019.03.001~~marenvres.2018.02.010

Legrand, E., Riera, P., Lutier, M., Coudret, J., Grall, J., & Martin, S. (2019). Grazers increase the sensitivity

of coralline algae to ocean acidification and warming. *Journal of Sea Research*, *148–149*, 1–7.

https://doi.org/10.1016/j.seares.2019.03.001

Legrand, E., Riera, P., Pouliquen, L., Bohner, O., Cariou, T., & Martin, S. (2018). Ecological

characterization of intertidal rockpools: Seasonal and diurnal monitoring of physico-chemical

parameters. *Regional Studies in Marine Science*, *17*, 1–10.

https://doi.org/10.1016/j.rsma.2017.11.003

Lorenzen, S. (2007). The limpet *Patella vulgata* L. at night in air: Effective feeding on *Ascophyllum*

nodosum monocultures and stranded seaweeds. *Journal of Molluscan Studies*, *73*(3), 267–274.

https://doi.org/10.1093/mollus/eym022

Mackey, K. R. M., Morris, J. J., Morel, F. M. M., & Kranz, S. A. (2015). Response of photosynthesis to

ocean acidification. *Oceanography*, *28*(2), 74–91.

Maneveldt, G. W., Wilby, D., Potgieter, M., & Hendricks, M. G. J. (2006). The role of encrusting coralline

algae in the diets of selected intertidal herbivores. *Journal of Applied Phycology*, *18*(3), 619–627.

https://doi.org/10.1007/s10811-006-9059-1

Martin, S., Charnoz, A., & Gattuso, J.-P. (2013). Photosynthesis, respiration and calcification in the

Mediterranean crustose coralline alga *Lithophyllum cabiochae* (Corallinales, Rhodophyta).

European Journal of Phycology, *48*(2), 163–172. https://doi.org/10.1080/09670262.2013.786790

Martin, S., Cohu, S., Vignot, C., Zimmerman, G., & Gattuso, J.-P. (2013). One-year experiment on the

physiological response of the Mediterranean crustose coralline alga, *Lithophyllum cabiochae*, to

elevated pCO$_2$ and temperature. *Ecology and Evolution*, *3*(3), 676–693.

https://doi.org/10.1002/ece3.475

847   Miller, C. A., & Kelley, A. L. (2021). Alkalinity cycling and carbonate chemistry decoupling in seagrass

848   mystify processes of acidification mitigation. *Scientific Reports*, *11:13500.*

849   https://doi.org/10.1038/s41598-021-92771-2

850   Morris, S., & Taylor, A. C. (1983). Diurnal and seasonal variation in physico-chemical conditions within

851   intertidal rock pools. *Estuarine, Coastal and Shelf Science*, *17*(3), 339–355.

852   https://doi.org/10.1016/0272-7714(83)90026-4

853   Nash, M. C., Diaz-Pulido, G., Harvey, A. S., & Adey, W. (2019). Coralline algal calcification: A

854   morphological and process-based understanding. *PLOS ONE*, *14*(9), e0221396.

855   https://doi.org/10.1371/journal.pone.0221396

856   Noisette, F., Egilsdottir, H., Davoult, D., & Martin, S. (2013). Physiological responses of three temperate

857   coralline algae from contrasting habitats to near-future ocean acidification. *Journal of*

858   *Experimental Marine Biology and Ecology*, *448*, 179–187.

859   https://doi.org/10.1016/j.jembe.2013.07.006

860   Paiva, F., Brennecke, D., Pansch, C., & Briski, E. (2021). Consistency of aquatic enclosed experiments: The

861   importance of scale and ecological complexity. *Diversity and Distributions*, *27*(3), 524–532.

862   Pan, T.-C. F., Applebaum, S. L., & Manahan, D. T. (2015). Experimental ocean acidification alters the

863   allocation of metabolic energy. *Proceedings of the National Academy of Sciences of the United*

864   *States of America*, *112*(15), 4696–4701. https://doi.org/10.1073/pnas.1416967112

865   Pansch, A., Winde, V., Asmus, R., & Asmus, H. (2016). Tidal benthic mesocosms simulating future climate

866   change scenarios in the field of marine ecology. *Limnology and Oceanography: Methods*, *14*(4),

867   257–267. https://doi.org/10.1002/lom3.10086

868   Pinheiro, J., Bates, D., & R-core. (2018). Package "nlme": Linear and Nonlinear Mixed Effects Models. In

869   *Cran-R.* [Computer software].

870   R Core Team. (2017). R: A language and environment for statistical computing. In *R: A language and*

871   *environment for statistical computing*. https://www.r-project.org/

872   Raven, J. A. (2011). Effects on marine algae of changed seawater chemistry with increasing atmospheric

873   CO_2. *Biology and Environment: Proceedings of the Royal Irish Academy*, *111B*(1), 1–17.

874   Riebesell, U., Czerny, J., von Bröckel, K., Boxhammer, T., Büdenbender, J., Deckelnick, M., Fischer, M.,

875   Hoffmann, D., Krug, S. A., Lentz, U., Ludwig, A., Muche, R., & Schulz, K. G. (2013). Technical Note:

876   A mobile sea-going mesocosm system – new opportunities for ocean change research.

877   *Biogeosciences*, *10*(3), 1835–1847. https://doi.org/10.5194/bg-10-1835-2013

878   Ries, J. B. (2011). Skeletal mineralogy in a high-CO_2 world. *Journal of Experimental Marine Biology and*

879   *Ecology*, *403*(1–2), 54–64. https://doi.org/10.1016/j.jembe.2011.04.006

880   Ries, J. B., Ghazaleh, M. N., Connolly, B., Westfield, I., & Castillo, K. D. (2016). Impacts of seawater

881   saturation state (ΩA=0.4–4.6) and temperature (10, 25°C) on the dissolution kinetics of whole-

882   shell biogenic carbonates. *Geochimica et Cosmochimica Acta*, *192*, 318–337.

883   https://doi.org/10.1016/j.gca.2016.07.001

884   Schaal, G., & Grall, J. (2015). Microscale aspects in the diet of the limpet Patella vulgata L. *Journal of the*

885   *Marine Biological Association of the United Kingdom*, *95*(6), 1155–1162.

886   https://doi.org/10.1017/S0025315415000429

887   Schulz, K. G., Bellerby, R. G. J., Brussaard, C. P. D., Büdenbender, J., Czerny, J., Engel, A., Fischer, M.,

888   Koch-Klavsen, S., Krug, S. A., Lischka, S., Ludwig, A., Meyerhöfer, M., Nondal, G., Silyakova, A.,

889   Stuhr, A., & Riebesell, U. (2013). Temporal biomass dynamics of an Arctic plankton bloom in

890   response to increasing levels of atmospheric carbon dioxide. *Biogeosciences*, *10*(1), 161–180.

891   https://doi.org/10.5194/bg-10-161-2013

892   Smith, S. V., & Key, G. S. (1975). Carbon dioxide and metabolism in marine environments. *Limnology and*

893   *Oceanography*, *20*(3), 493–495. https://doi.org/10.4319/lo.1975.20.3.0493

894 Spisla, C., Taucher, J., Bach, L. T., Haunost, M., Boxhammer, T., King, A. L., Jenkins, B. D., Wallace, J. R.,

895   Ludwig, A., Meyer, J., Stange, P., Minutolo, F., Lohbeck, K. T., Nauendorf, A., Kalter, V., Lischka,

896   S., Sswat, M., Dörner, I., Ismar-Rebitz, S. M. H., … Riebesell, U. (2021). Extreme levels of ocean

897   acidification restructure the plankton community and biogeochemistry of a temperate coastal

898   ecosystem: A mesocosm study. *Frontiers in Marine Science*, *7:611157*.

899   https://www.frontiersin.org/articles/10.3389/fmars.2020.611157

900 Stumpp, M., Hu, M. Y., Casties, I., Saborowski, R., Bleich, M., Melzner, F., & Dupont, S. (2013). Digestion

901   in sea urchin larvae impaired under ocean acidification. *Nature Climate Change*, *3*(12), 1044–

902   1049. https://doi.org/10.1038/nclimate2028

903 Sulpis, O., Jeansson, E., Dinauer, A., Lauvset, S. K., & Middelburg, J. J. (2021). Calcium carbonate

904   dissolution patterns in the ocean. *Nature Geoscience*, *14*(6), Article 6.

905   https://doi.org/10.1038/s41561-021-00743-y

906 Sulpis, O., Lauvset, S. K., & Hagens, M. (2020). Current estimates of K1* and K2* appear inconsistent

907   with measured CO_2 system parameters in cold oceanic regions. *Ocean Science*, *16*(4), 847–862.

908   https://doi.org/10.5194/os-16-847-2020

909 Torres, O., Kwiatkowski, L., Sutton, A. J., Dorey, N., & Orr, J. C. (2021). Characterizing mean and extreme

910   diurnal variability of ocean CO_2 system variables across marine environments. *Geophysical*

911   *Research Letters*, *48*(5), e2020GL090228. https://doi.org/10.1029/2020GL090228

912 Widdicombe, S., Dupont, S., & Thorndyke, M. (2010). Laboratory experiments and benthic mesocosm

913   studies. In *Guide to best practices for ocean acidification research and data reporting. U.*

914   *Riebesell, V. J. Fabry, L. Hansson and J.-P. Gattuso.* Publications Office of the European Union.

915 Williamson, C. J., Perkins, R., Voller, M., Yallop, M. L., & Brodie, J. (2017). The regulation of coralline algal

916   physiology, an in situ study of *Corallina officinalis* (Corallinales, Rhodophyta). *Biogeosciences*,

917   *14*(19), 4485–4498. https://doi.org/10.5194/bg-14-4485-2017

918   Yamamoto, S., Kayanne, H., Terai, M., Watanabe, A., Kato, K., Negishi, A., & Nozaki, K. (2012). Threshold

919   of carbonate saturation state determined by CO_2 control experiment. *Biogeosciences*, *9*(4),

920   1441–1450. https://doi.org/10.5194/bg-9-1441-2012

921

Formatted: Bibliography, Left

1 **Figures with legends -**
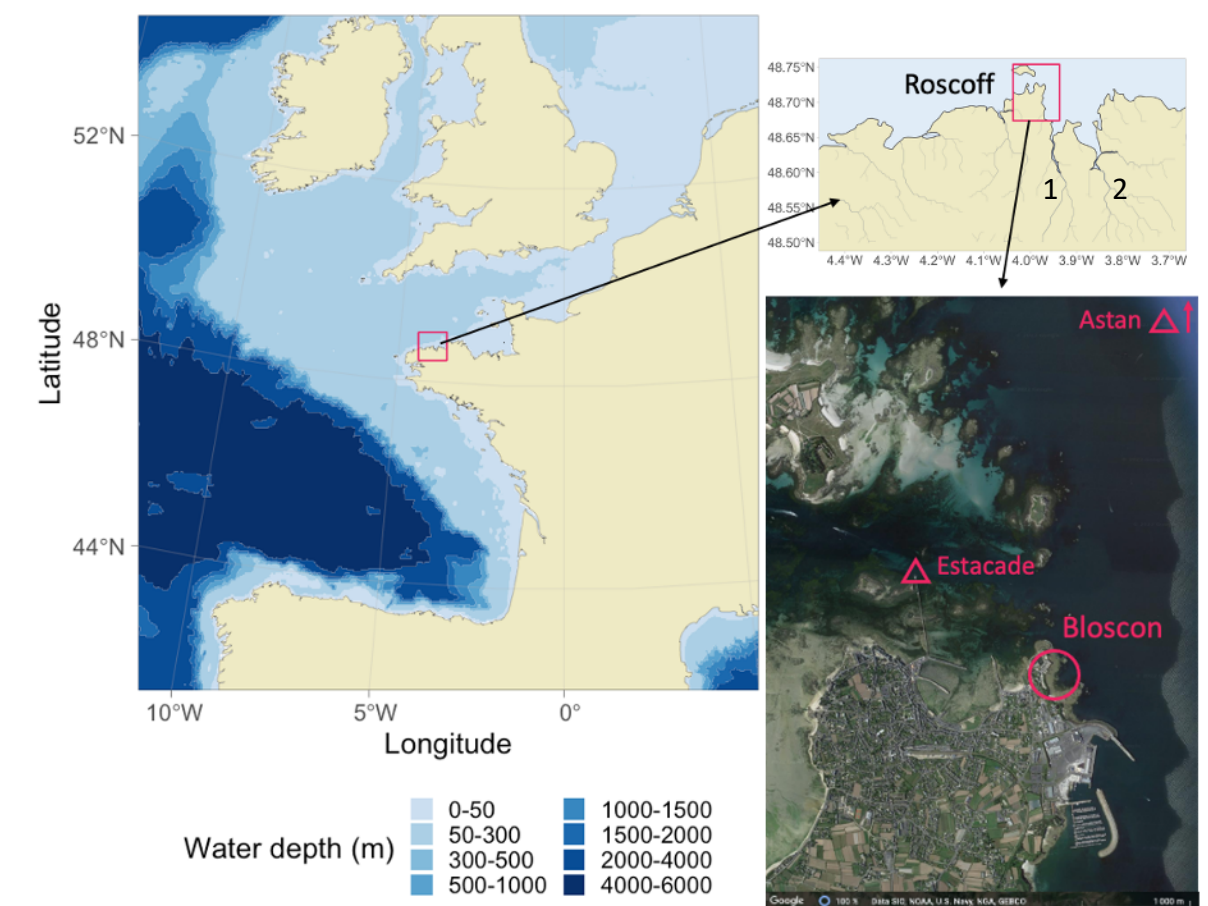
Figure 1 - Field site location on a map of Europe (**left**). The study site (Bloscon) is located in Roscoff, Brittany, France (**right**, top: river mapping data from *HydroSHEDS,* **1**. Penzé river and **2**. Morlaix river; bottom: satellite image from ~~*Google Earth*~~: earth.google.com/web/, acquired in June 2022). The SOMLIT stations Astan and Estacade are indicated with triangles (www.somlit.fr).
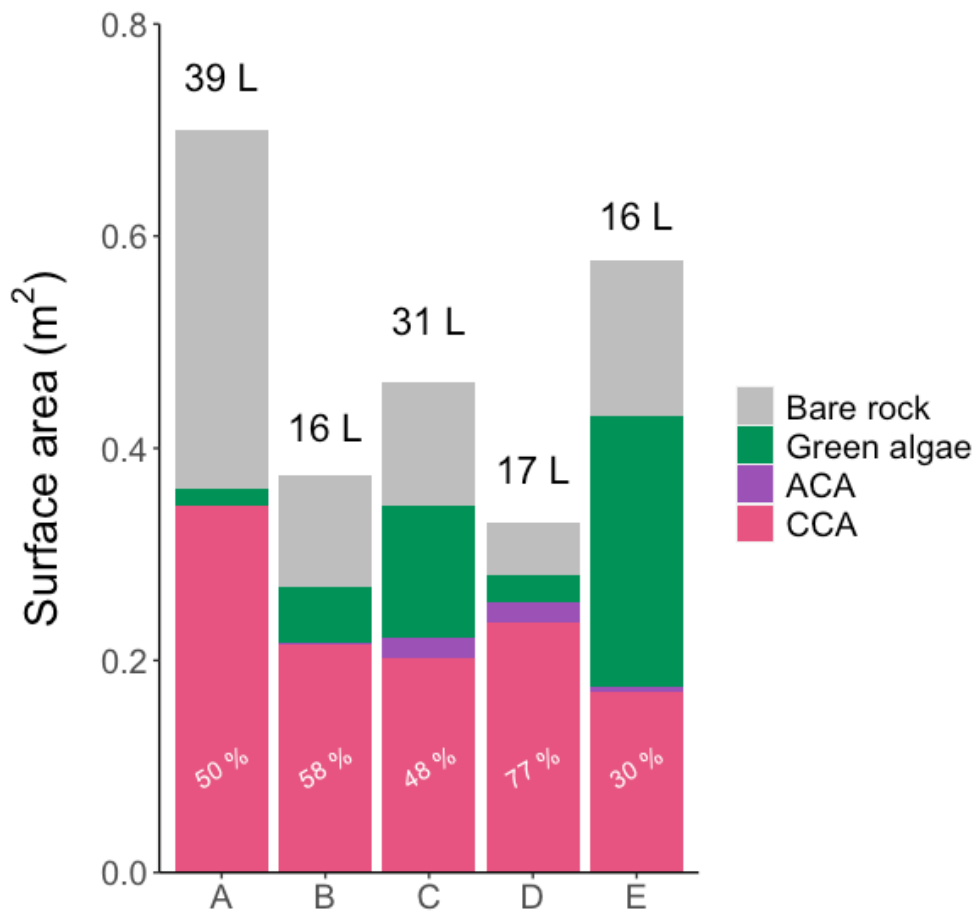
Figure 2 - Pool area, volume and coverage - Surface of the five pools (A-E, September 2020) covered by crustose coralline algae (CCA, pink), articulated coralline algae (ACA, purple) and green algae (green) or free of algae ("bare rock", grey). The length of the bars represents total pool surface area (m²) and the volume of each pool (L) is indicated above. The relative coverage (%) of calcifying algae (ACA + CCA) in each pool is given. Details for the other seasons are available in **Supp. Mat. Pools Fig. SP1** and **SP2**.

13 **Figure 3 - Composite daily pool conditions and biological activity for all pools. A) temperature**
14 (°C), **salinity and oxygen concentration** (mg L^{-1}) **and Photosynthetically Active Radiation** (PAR,
15 μmol m^{-2} s^{-1}), **B) pH$_T$, Total Alkalinity** (TA, μmol kg^{-1}), **pCO$_2$** (μatm), **dissolved inorganic carbon**
16 (DIC, μmol kg^{-1}) **and aragonite saturation state** (Ω_a), and **C) DIC and O$_2$-derived NCP or CR**
17 (mmol C or O m^{-2} hr^{-1}) **and NCC** (mmol CaCO$_3$ m^{-2} hr^{-1}). Colors represent seasons (**A:** blue for
18 February, orange for April, red for September) and treatment (**B and C**: purple for "present" and green
19 for "future"). Horizontal dotted grey lines represent the mean values of the adjacent ocean. Curves
20 were fitted by season for PAR and for diurnal NCP and NCC using a local polynomial regression
21 (*loess*) with 95% confidence interval. Number of observations: n = 1551 for temperature, salinity and
22 pH$_T$, n = 1169 for oxygen concentration (data recorded < 22 mg L^{-1}) and n = 632 (hourly data) for the
23 carbonate chemistry parameters, NCC and NCP or CR (**B**). All pools are shown.

C
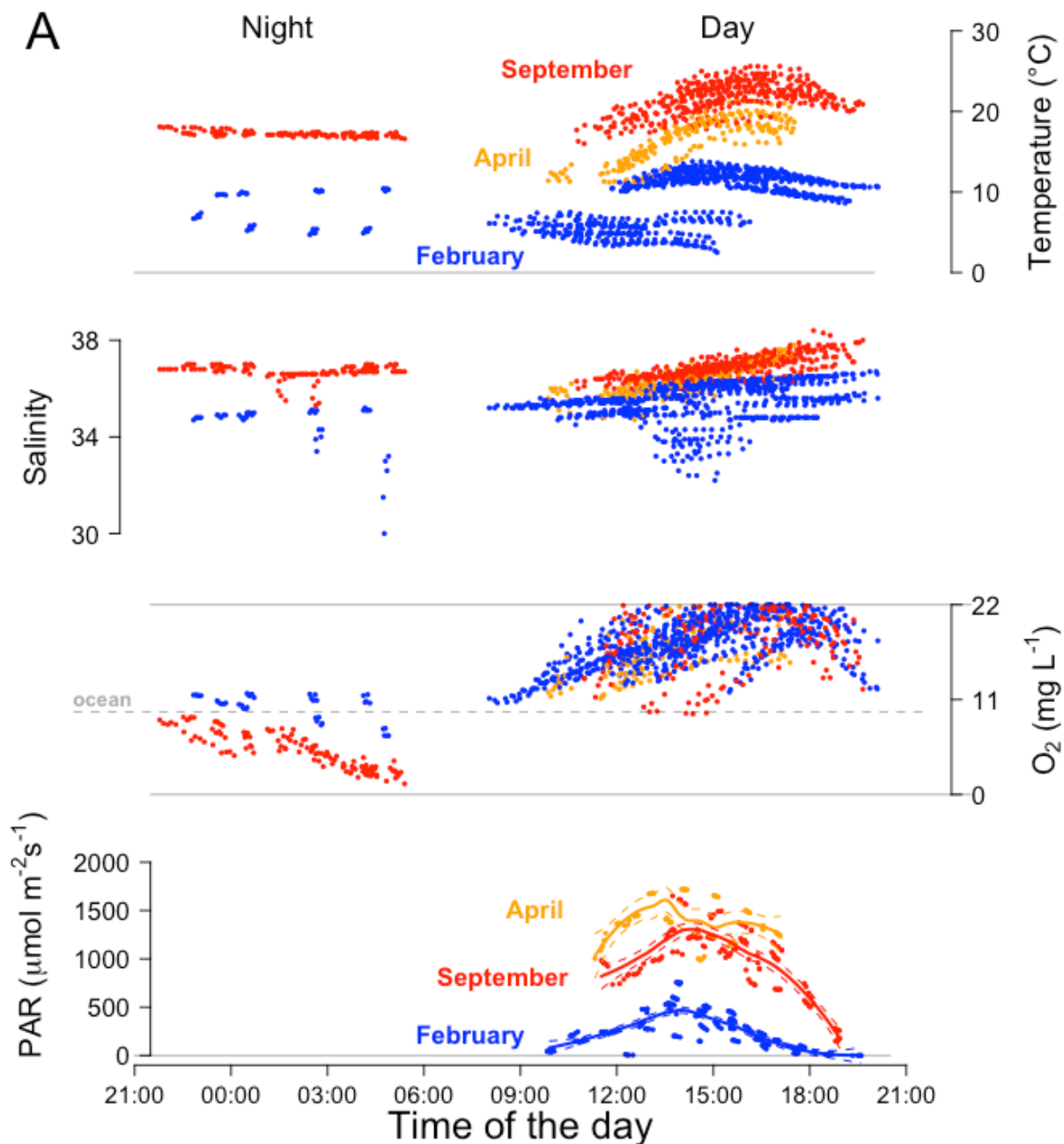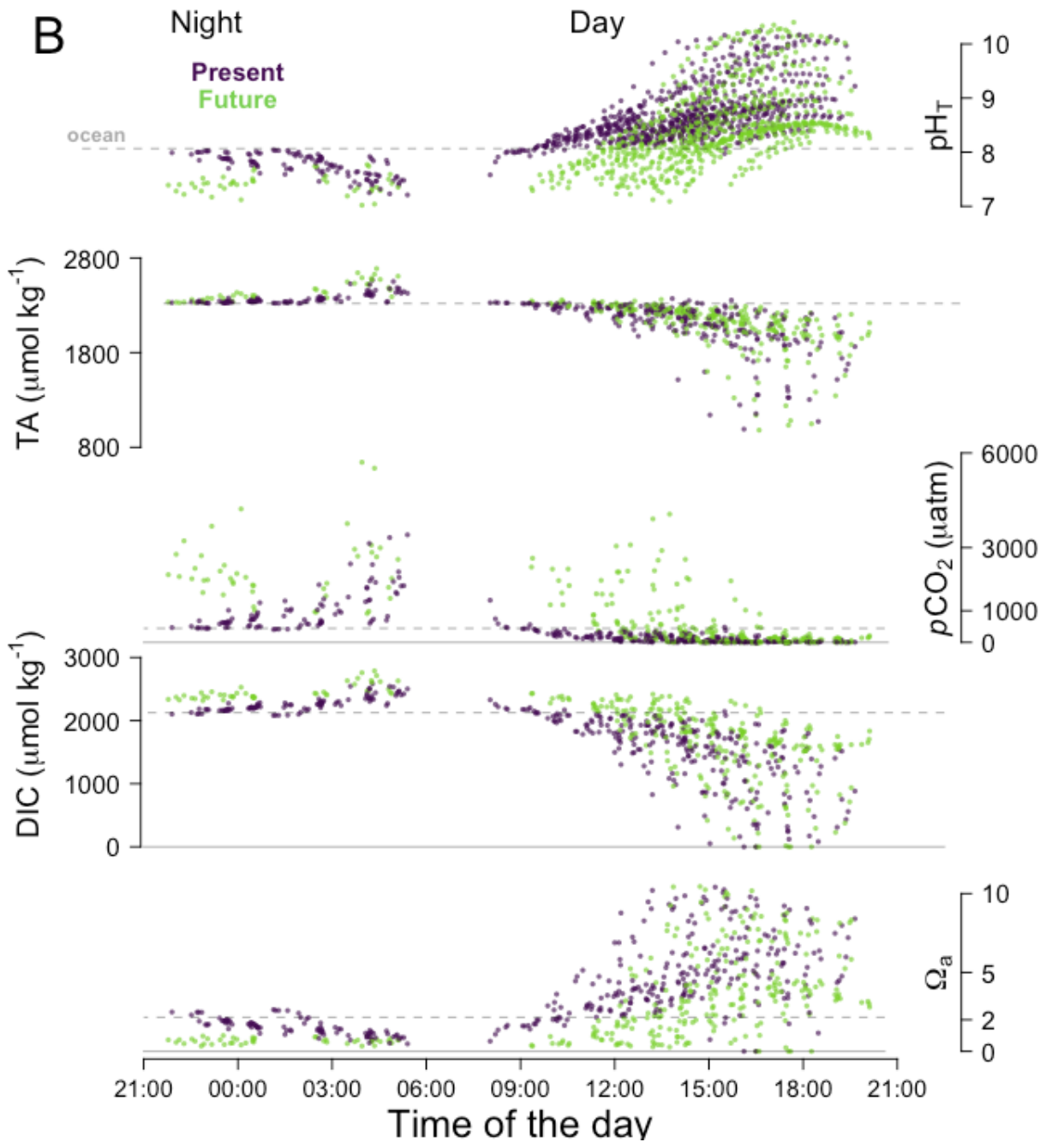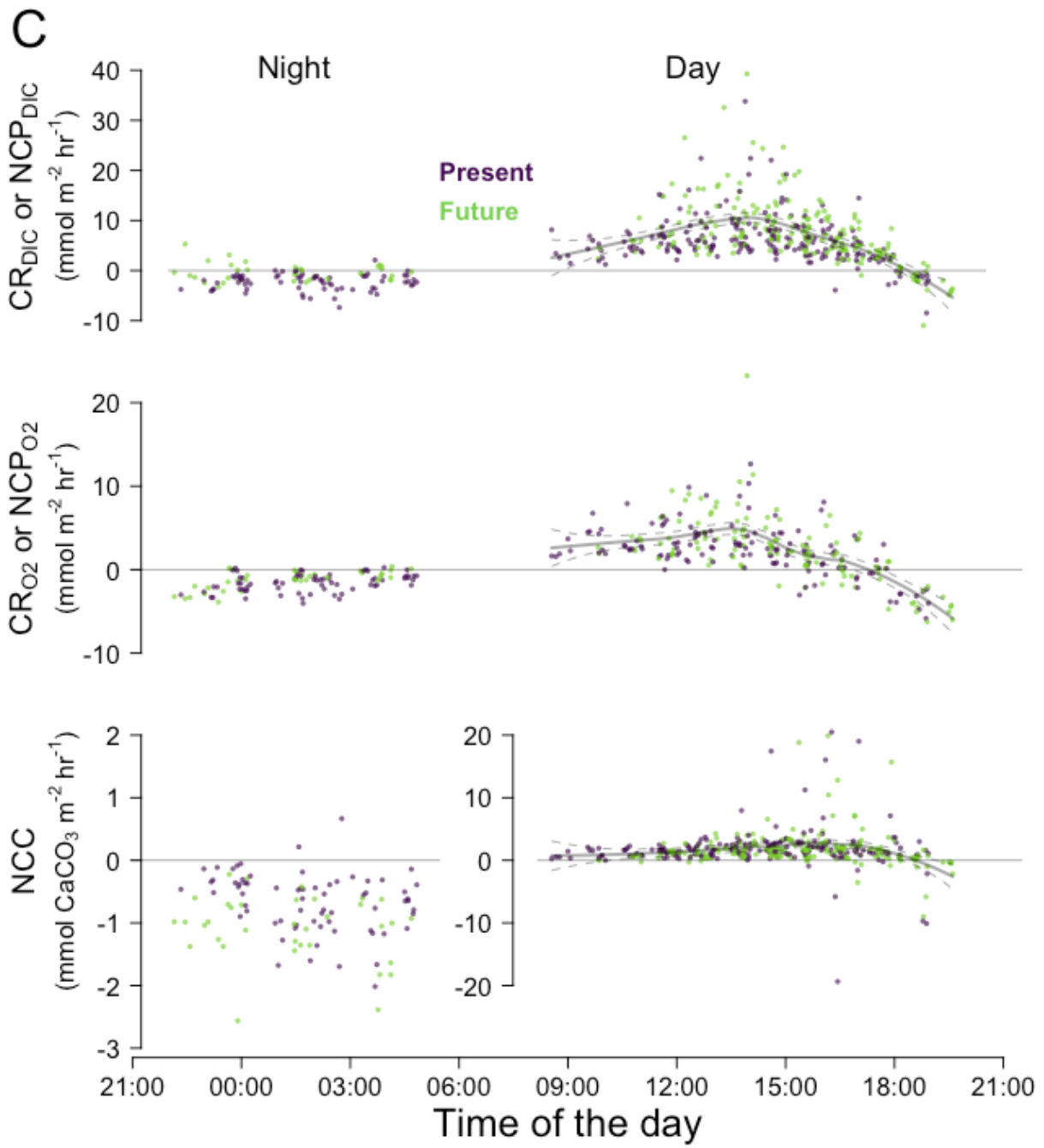
28 **Figure 4 – A) O$_2$-derived (white boxes) and DIC-derived (colored boxes) NCP$_{lm}$ (mmol m^{-2} hr^{-1}),**
29 **and B) NCC$_{lm}$ (mmol CaCO$_3$ m^{-2} hr^{-1}) during the day and night (shaded areas), by season and**
30 **by treatment** (purple for "present" and green for "future") – Rates are presented as boxplots showing
31 median, 1st and 3rd quartile and 1.5 inter-quartile range (bars), with overlayed individual observations
32 (round symbols). Individual rates were calculated for each pool, each tide and each treatment: n = 50
33 (FEB-day), n = 10 (FEB-night), n = 10 (APR-Day), n = 25 (SEP-Day), n = 20 (SEP-Night). Seasons:
34 FEB for winter (pooled February 2020 and 2021), APR for spring (April 2021) and SEP for summer
35 (pooled September 2020 and 2021). *Note that for NCC$_{lm}$, nights (<0) and days (>0) have different y-*
36 *axis scales for better visualization of night differences. Statistical details of the linear regressions can*
37 *be found in the corresponding **Supplementary Materials**. For O$_2$-derived NCP$_{lm}$, in September, three*
38 *rates were out of the range plotted and their values are indicated next to the small arrow.*
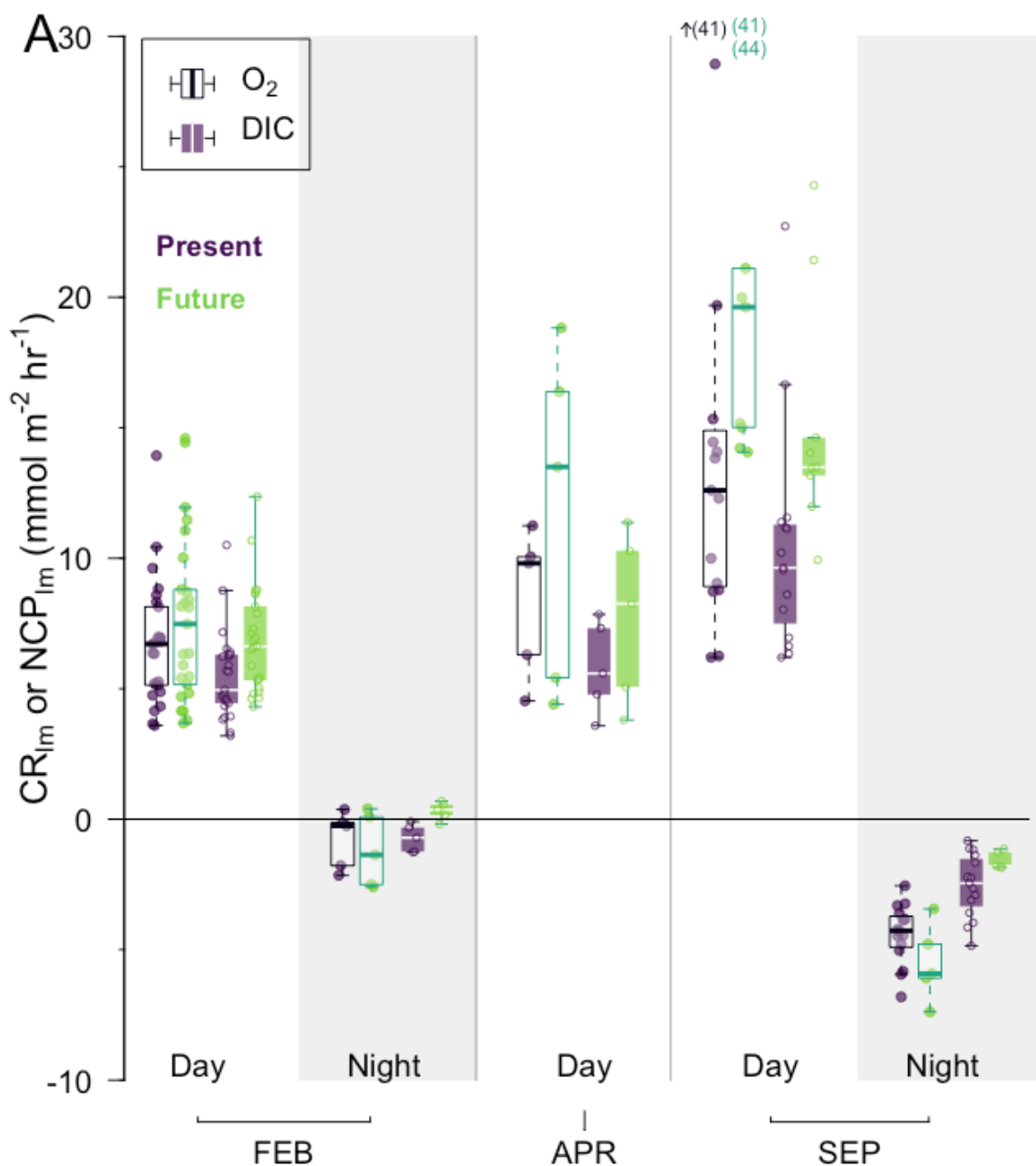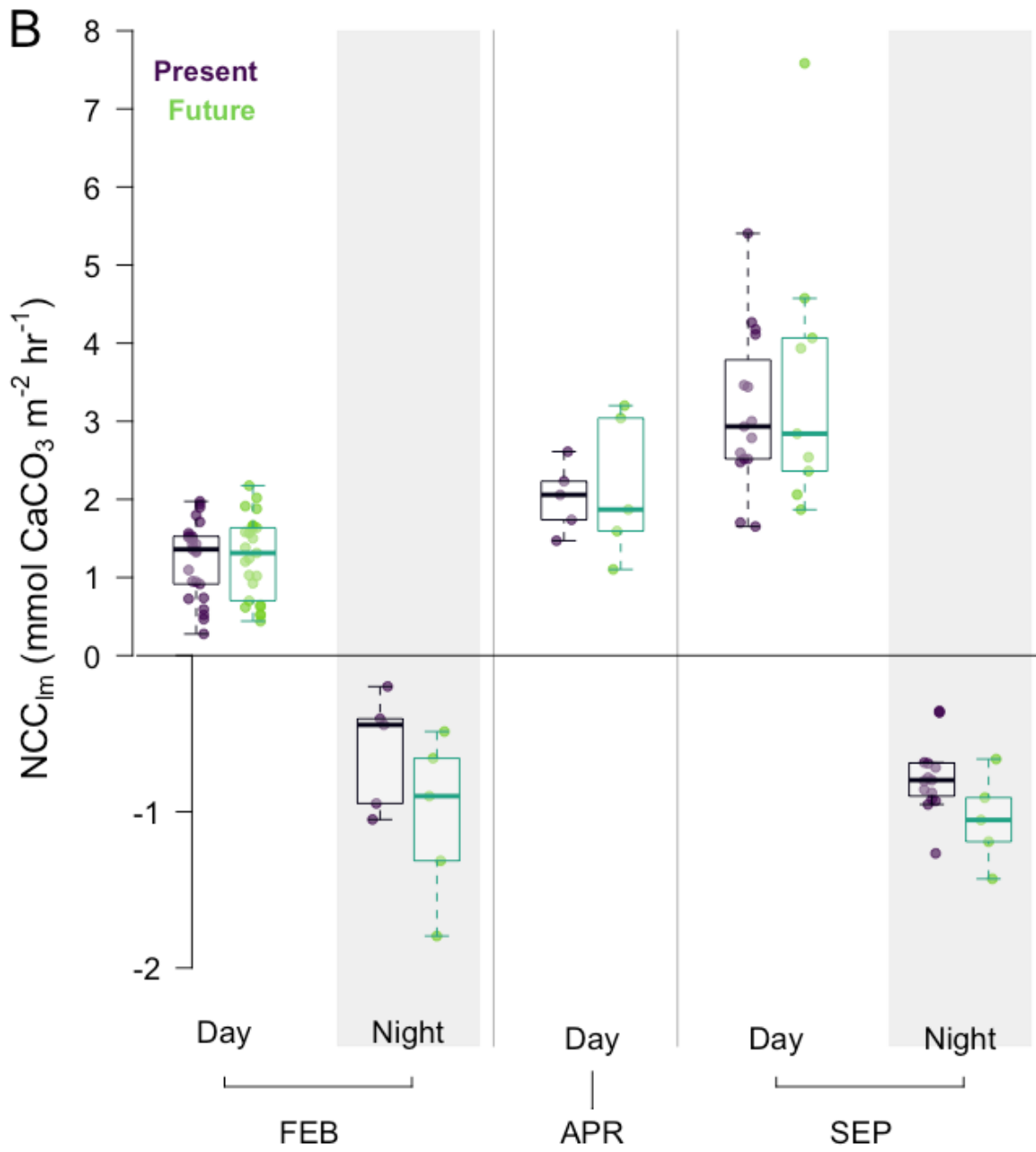
Figure 5 – Community production budget: CPB [1], and calcification budget: CCB (upper right panel, mmol CaCO₃ m⁻² hr⁻1) by treatment (purple for "present" and green for "future") for each pool and season (same legend as Fig. 4). CPB >0 if diurnal NCP > nocturnal respiration and CCB > 0 if diurnal NCC > nocturnal dissolution. CPB was estimated three different ways: from O₂-derived NCP (bars), from DIC-derived NCP (round symbols) and from nocturnal O₂-derived CR combined with diurnal DIC-derived NCP ("mixed", vertical segments). **The bottom panels present the change (%) of diel production (ΔCPB: left) and diel calcification (ΔCCB: right) due to CO₂ addition.** Positive ΔCPB indicates a fertilization effect due to the CO₂ addition; negative ΔCCB is expected if the CO₂ addition decreases net calcification/increases net dissolution. All three methods to estimate CPB indicate a fertilization effect in summer.

50
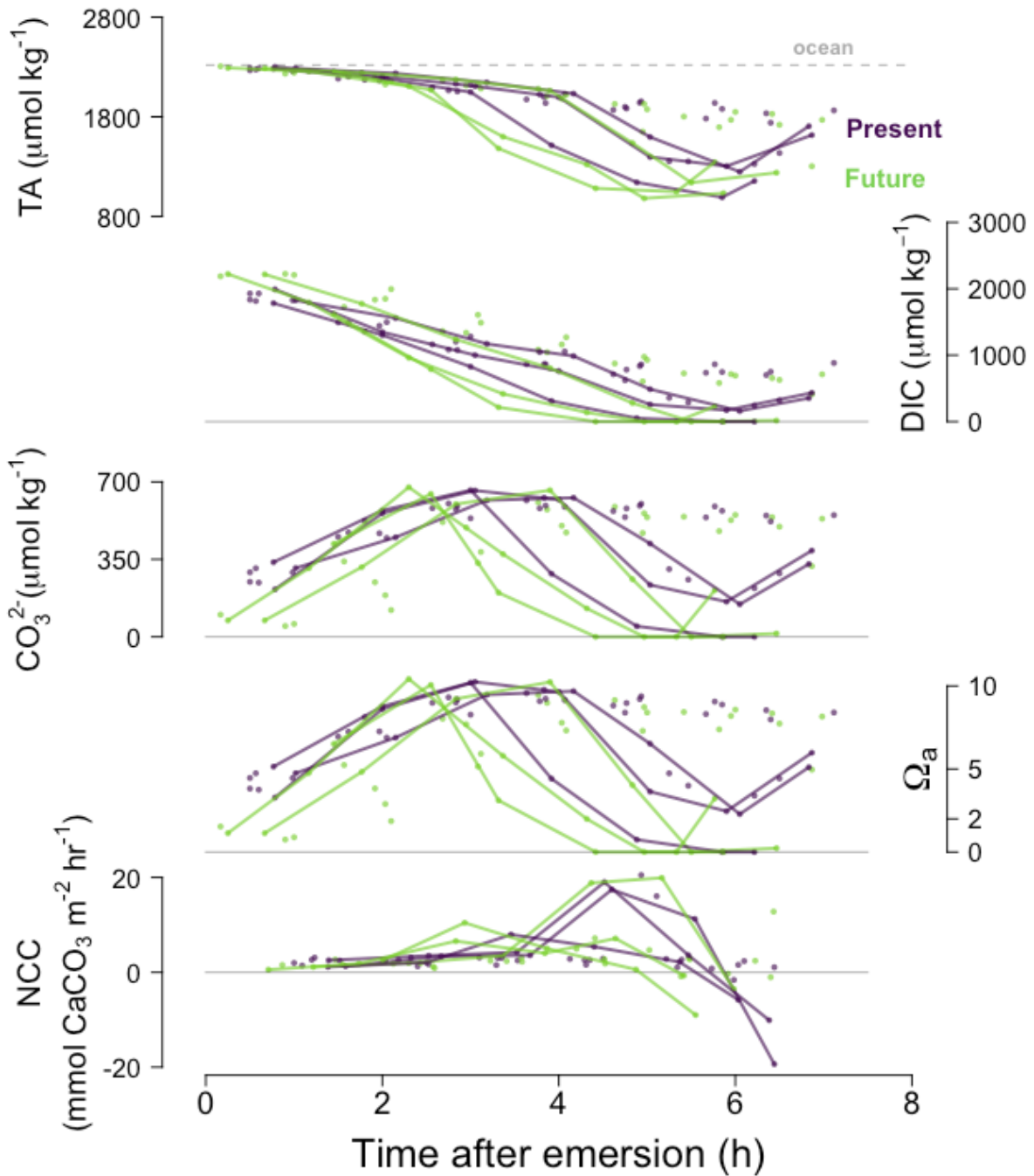
Figure 6 - Time series for September 2020 diurnal data only: A) Total Alkalinity (TA, μmol kg⁻¹), dissolved inorganic carbon, CO_3^{2-} concentration (μmol kg⁻¹), aragonite saturation state (Ω_a) and NCC (mmol m⁻² hr⁻¹) with time after emersion, by treatment (purple for "present" and green for "future"). The lines in bold represent individual pools C and E that switched from calcification to dissolution when pH_T was still above 9. A similar figure in **Supp. Mat. (Fig. S4)** shows that sunset/irradiance are not correlated with the sudden change towards dissolution.

57
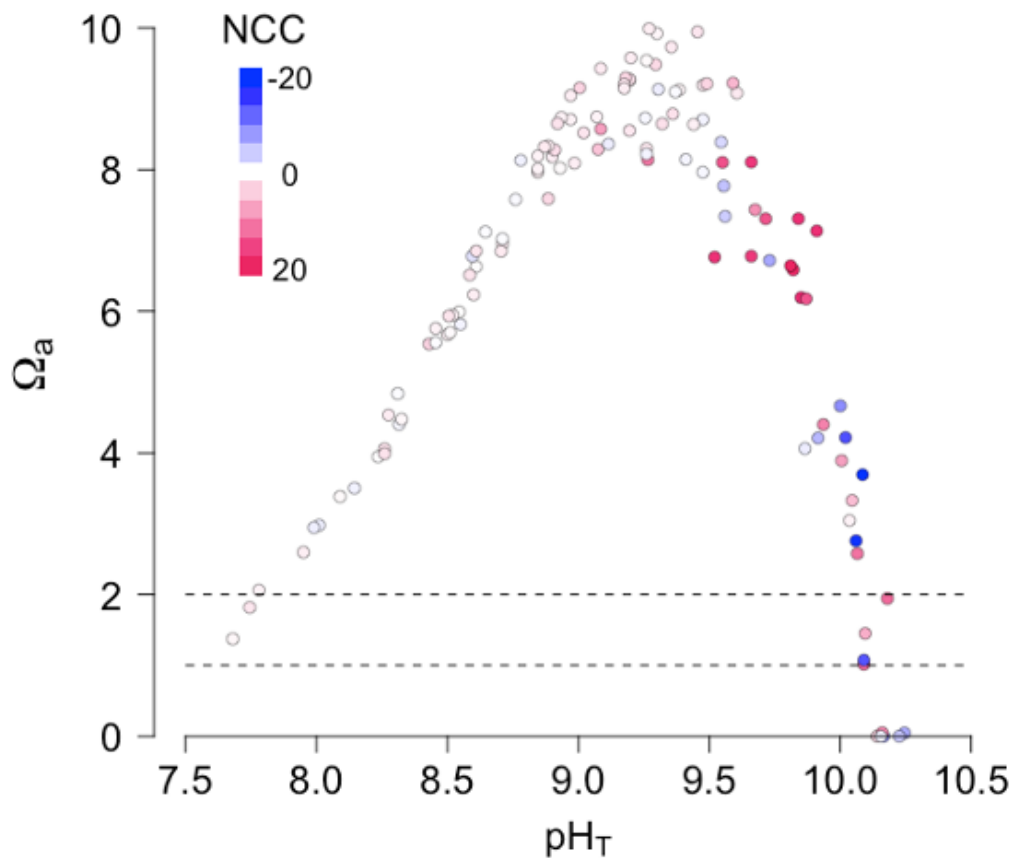
Figure 7 – At very high pH there was both fast net calcification (red) and rapid net dissolution
(blue): In some extreme cases, pH_T was not a good indicator or seawater saturation state (Ω_a). Selected
dataset of diurnal low-tide emersion periods from September 2020. Colors represent NCC (in mmol
$CaCO_3$ m^{-2} hr^{-1}, as presented in Fig. 3C). Dashed horizontal lines represent saturation state for
aragonite ($\Omega_a = 1$) and for high-Mg calcite ($\Omega_a = 2$).